

Environmental Controls on Observed Spatial Variability of Soil Pore Water Geochemistry in Small Headwater Catchments Underlain with Permafrost

Nathan Alec Conroy,^{1*} Jeffrey M. Heikoop,¹ Emma Lathrop,^{1,2} Dea Musa,¹ Brent D. Newman,¹ Chonggang Xu,¹ Rachael E. McCaully,³ Carli A. Arendt,³ Verity G. Salmon,⁴ Amy Breen,⁵ Vladimir Romanovsky,⁶ Katrina E. Bennett,¹ Cathy J. Wilson,¹ and Stan D. Wullschlegel⁴

¹Earth and Environmental Sciences Division, Los Alamos National Laboratory, Bikini Atoll Road, Los Alamos, New Mexico, 87545, [USA](#)

²Center for Ecosystem Science and Society, Department of Biological Sciences, Northern Arizona University, Flagstaff, AZ, 86011, USA

³Department of Marine Earth and Atmospheric Sciences, North Carolina State University, Raleigh, North Carolina, 27695, [USA](#)

⁴Biological and Environmental Systems Science Division and Climate Change Science Institute, Oak Ridge National Laboratory, Oak Ridge, Tennessee, 37831, [USA](#)

⁵International Arctic Research Center, P.O. Box 757340, University of Alaska, Fairbanks, Alaska 99775-7340, USA

⁶Geophysical Institute, University of Alaska Fairbanks, Fairbanks, Alaska, 99775, [USA](#)

Correspondence to: Nathan Alec Conroy (nconroy@lanl.gov)

Abstract. Soil pore water (SPW) chemistry can vary substantially across multiple scales in Arctic permafrost landscapes. The magnitude of these variations and their relationship to scale are critical considerations for understanding current controls on geochemical cycling and for predicting future changes. These aspects are especially important for Arctic change modelling where accurate representation of sub-grid variability may be necessary to predict watershed scale behaviours. Our research goal ~~was-is~~ to characterize intra- and inter-watershed soil water geochemical variations at two contrasting locations in the Seward Peninsula of Alaska, USA. We then attempt to ~~establish which identify the key factors environmental factors were important for~~ controlling concentrations of important pore water solutes in these systems. The SPW geochemistry of 18 locations spanning two small Arctic catchments were examined for spatial variability and its dominant environmental controls. The primary environmental controls considered were vegetation, soil moisture/redox condition, water/soil interactions and hydrologic transport, and mineral solubility. The sampling locations varied in terms of vegetation type and canopy height, presence or absence of near-surface permafrost, soil moisture, and hillslope position. Vegetation was found to have a significant impact on SPW ~~NO₃NO₂⁻ concentrations, associated with the localized presence of nitrogen-fixing alders and mineralization and nitrification of leaf litter from tall willow shrubs. The elevated NO₃NO₂⁻ concentrations were~~ however, frequently equipoised by increased microbial denitrification in regions with sufficient moisture to support it. Vegetation also had an observable impact on soil moisture sensitive constituents, but the effect was less significant. The redox conditions in both catchments were generally limited by Fe reduction, seemingly well-buffered by a cache of amorphous Fe hydroxides, with the most reducing conditions found at sampling locations with the highest soil moisture content. Non-redox-sensitive cations were affected by a wide variety of water-soil interactions that affect mineral solubility and transport. Identification of the dominant controls on current SPW hydrogeochemistry allows for qualitative prediction of future geochemical trends in small Arctic catchments that are likely to experience warming and permafrost thaw. As source areas for geochemical fluxes to the broader Arctic hydrologic system, geochemical

Formatted: Subscript

Formatted: Subscript

40 processes occurring in these environments are particularly important to understand and predict with regards to such
41 environmental changes.

42 1. Introduction

43 Permafrost thaw in the Arctic is causing significant changes to landscape structure (Kokelj and Jorgenson, 2013;
44 Rowland et al., 2010), hydrology (Hiyama et al., 2021; Kurylyk et al., 2021; Liljedahl et al., 2016; Vonk, Tank, and
45 Walvoord, 2019; Walvoord and Kurylyk, 2016), vegetation (Lara ~~et al., Nitze, Grosse, and McGuire~~, 2018; Myers-
46 Smith et al., 2011; Sturm, Racine, and Tape, 2001; K. D. Tape ~~et al., Hallinger, Welker, and Ruess~~, 2012; ~~K-~~Tape,
47 Sturm, and Racine, 2006;), and biogeochemistry (O'Donnell et al., 2021; Frey and McClelland, 2009; Salmon et al.,
48 2019; Vonk, Tank, and Walvoord, 2019). The integrated hydrogeochemical effects of these environmental changes
49 are already apparent in the chemistry of the large Arctic rivers, where fluxes of carbon and nutrients are increasing,
50 leading to enhanced nutrient loadings, with strong implications for the global carbon cycle (Bring et al., 2016; Fuchs
51 et al., 2020; McClelland et al., 2016). While the watershed areas of large Arctic rivers are vast, recent studies suggest
52 that solute concentrations in these large rivers are likely controlled by solute generation processes occurring at much
53 smaller scales (Harms and Ludwig, 2016; Koch ~~et al., Runkel, Striegl, and McKnight~~, 2013; Shogren et al., 2019;
54 Vonk et al., 2015).

55 While there is a rapidly growing body of literature focused on observing and understanding environmental changes
56 over time with further Arctic warming, relatively few studies directly address the existing spatial variability, within
57 catchments or across catchments, and we are not aware of any studies that have combined field observations with
58 thermodynamic modelling in an effort to understand the causes of the existing spatial variability. Therefore, we have
59 a limited understanding of the key environmental controls on the spatial distribution of soil pore water solute
60 concentrations. In this study, we quantitatively evaluate the spatial variability of soil pore water (SPW) geochemistry
61 within and between two distinct catchments underlain with permafrost, and then seek to identify the source of the
62 observed spatial variability.

63 This study takes advantage of a scientifically diverse array of observations and datasets made available by the Next
64 Generation Ecosystem Experiment (NGEE) Arctic project, sponsored by the US Department of Energy Office of
65 Science. Most of the locations studied herein were selected by the NGEE Arctic project to provide co-located
66 measurements in a wide range of vegetation types, nested within representative hillslopes and catchments. Although
67 selected largely to represent a range of vegetation structure, such as shrub abundance and canopy height, these
68 locations also have considerable variability in other environmental parameters including, but not limited to: soil
69 moisture and temperature, presence or absence of near-surface permafrost, and maximum observed thaw depth (**Table**
70 **1** and **Table 2**). The vegetation-delineated sampling approach ~~presented here~~ provides an opportunity to not only
71 quantify the biogeochemical variability of SPW in Arctic environments, but also to investigate the root causes of that
72 observed variability. Data from additional sampling locations, available from a ~~collaborative-co-located~~ study, were
73 also utilized when possible.

74 Our overarching hypothesis is that vegetation-type and hillslope position are the dominant controls on spatial
75 variability of SPW geochemistry at the NGEE Arctic field sites located on the Seward Peninsula. Vegetation-type

76 seems likely to have a significant effect on SPW geochemistry both directly and indirectly. Indirect effects would
77 include vegetation canopy impacts on soil moisture (through evapotranspiration and snow trapping). Direct effects of
78 vegetation would include nutrient cycle changes resulting from the annual deposition of plant litter. Such a direct
79 effect can be augmented at sites populated by alder shrubs due to this genus of deciduous shrubs ability to form a
80 symbiotic relationship with nitrogen-fixing *Frankia*, which they host in underground root nodules. Nitrogen fixation
81 associated with alders has previously been shown to accelerate local nitrogen cycling (Binkley et al., 1992; Clein and
82 Schimel, 1995; Bühlmann et al., 2014). Directly, through the increased cycling of some solutes (e.g. increased nitrogen
83 concentrations in the vicinity of alders, which add nitrogen to soils via a symbiotic relationship with nitrogen fixing
84 bacterium; Salmon et al., 2019), and indirectly, through effects on soil moisture (i.e. evapotranspiration and trapping
85 of snow). Soil moisture will also affect SPW geochemistry, particularly of redox sensitive species, by limiting oxygen
86 diffusion and thus controlling which regions develop anoxic/reducing geochemical conditions. Soil moisture impacts
87 will likely be correlated with vegetation-type as well as hillslope position, and the presence or absence of perching
88 layers, including permafrost, all of which impact the vertical and horizontal drainage characteristics of a watershed.
89 Chemical species that are not redox-sensitive or controlled by biogeochemical reactions are likely to be
90 ~~effeted~~affected by transport, solubility, and water/sediment/organic matter interactions, and therefore largely
91 controlled by hillslope position as well as soil moisture.

92 Identifying the dominant controls on solute concentration variability within each catchment and across catchments
93 will facilitate better projections of future soil pore hydrogeochemistry in permafrost landscapes, and how these
94 signatures are related to changing soil moisture and increasing ~~in~~ tundra shrub abundance in a changing Arctic (Bring
95 et al., 2016; Myers-Smith et al., 2011; Prowse ~~et al.~~, Bring, Mård, and Carmack, 2015; Salmon et al., 2019; Sturm et
96 al., 2001; ~~K. D.~~ Tape et al., 2012; ~~K.~~ Tape et al., 2006; Wrona et al., 2016, 2016). Arctic warming and associated
97 permafrost thaw will increase hydrological connectedness between terrestrial and aquatic environments through
98 deepening of the active layer and the formation of deeper, more coherent groundwater flow paths (Bring et al., 2016;
99 Harms and Jones, 2012; Prowse, ~~Bring, Mård, Carmack,~~ et al., 2015a; Prowse, ~~Bring, Mård, and Carmack,~~ et al.,
100 2015b). Meanwhile, changes in hydrogeochemical signatures in larger Arctic rivers are likely to originate in smaller
101 catchments (McClelland et al., 2016; Prowse ~~et al.~~, ~~Bring, Mård, and Carmack,~~ 2015; Shogren et al., 2019; Spence,
102 ~~et al., Kokelj, McCluskie, and Hedstrom,~~ 2015). In this sense, changes in hydrogeochemistry in small Arctic
103 catchments not only impact hydrogeochemistry at much larger scales, but also prognosticate the future
104 hydrogeochemistry of larger Arctic rivers.

105 2. Methods

106 2.1 Site Descriptions

107 This study focuses on two sites with permafrost on the Seward Peninsula of western Alaska, the Teller-27 Catchment
108 and the Kougarak-64 Hillslope (**Figure 1**). The Teller-27 Catchment, henceforth “Teller,” is a small (~2.25 km²)
109 headwater catchment located west of mile marker 27 along the Nome-Teller Highway northwest of Nome, Alaska.
110 The Kougarak-64 Hillslope, henceforth “Kougarak,” is a hillslope (~2.0 km²) located west of mile marker 64 along

Formatted: Font: Italic

Formatted: Font: Not Italic

Formatted: Superscript

Formatted: Superscript

111 the Nome-Taylor Highway northeast of Nome, Alaska. We utilized data from “intensive stations” at both Teller and
112 Kougarak where concentrated, multi-year, co-located observations of soil water chemistry, vegetation characteristics,
113 soil moisture and temperature, and other measurements have been collected as part of the NGEE Arctic Research
114 Project. These are identified as TL# (Teller Station #) or KG# (Kougarak Station #) in **Figure 2** and **Figure 3**,
115 respectively. It should be noted that Teller and Kougarak are not “paired watersheds” in the classical sense, differing
116 in only one major characteristic, which provides the basis for comparison. Instead, Teller and Kougarak differ in many
117 respects and are both representative of the broad range of hillslope conditions common on the Seward Peninsula.
118 Detailed descriptions of Teller and Kougarak have been published previously (Jafarov et al., 2018; Léger et al., 2019;
119 Philben et al., 2019, 2020; Salmon et al., 2019; Yang et al., 2020), therefore, only the catchment characteristics that
120 are probable sources of variability in SPW chemistry will be highlighted here.

121 Teller is a discrete catchment with a well-defined central drainage, a vertical declivity of approximately 200 m, and a
122 catchment area of approximately 2.25 km². Temperature probes, soil pits, coring activities, and geophysical
123 interpretations at Teller have confirmed the catchment is underlain with discontinuous permafrost (Léger et al., 2019).
124 The upper shoulder of Teller (near Station 5, **Figure 2** and **Figure 5**) is underlain with near-surface permafrost and
125 appears to be a degraded peat plateau. The resultant microtopography of the degraded peat and the shallow perching
126 horizon caused by the permafrost creates a landscape of unsaturated peat mounds surrounded by ponds and saturated
127 soils. Downslope of the peat plateau, the Teller hillslope has highly variable soil moisture and vegetation (**Table 1**).
128 The microtopography within the lower footslope looks similar to the upper shoulder, but the peat appears more
129 severely degraded and the cause of the perched water table is less clear. Léger et al. (2019) suggest the presence of
130 permafrost at a depth of 1 – 2 m at Teller Station 9 (**Figure 2**), but the perching could also be caused by a layer of silt,
131 at a depth of approximately 30 cm (Graham et al., 2018). The full extent of permafrost and silt in this region of the
132 catchment remains unknown, but the thaw depth in July 2018 was greater than 1 m and maintained a perched water
133 table (Philben et al., 2020), suggesting perching could be the result of silt rather than permafrost. Vegetation type,
134 moisture content, permafrost extent, and hillslope position for all Teller Stations are summarized in **Table 1**.

135 Kougarak differs in many ways from Teller, although both have characteristics that are typical of hillslopes on the
136 Seward Peninsula. Kougarak is a convex hillslope, with a vertical declivity of approximately 70 meters. The study
137 area at Kougarak is approximately 2.0 km². Soil temperature measurements at Kougarak suggest that the vast majority
138 of the site is underlain by shallow continuous permafrost (Romanovsky, Cable, and Dolgikh, 2020a); Kougarak
139 Station 5 is an exception, where the permafrost is deeper (Romanovsky et al., 2020a). The upper shoulder of Kougarak
140 is a well-drained rocky outcrop composed of metagranitic rock (Hopkins et al., 1955; Till, Dumoulin, Werdon, and
141 Bleick, 2011). Saturated soils are not prevalent until the footslope and the lower backslope, where Kougarak Stations
142 2, 11, 10, 1, and 6 are situated (**Figure 3**). The lower backslope is characterized by persistent saturation between
143 ubiquitous tussocks, formed by the tussock cotton grass *Eriophorum vaginatum*. The tussock-lichen tundra at
144 Kougarak introduces microtopography and spatially variable saturation; in this sense, the Kougarak tussocks are
145 analogous to the peat mounds and hummocks at Teller, but on different spatial scales and formed by different
146 processes. Kougarak has numerous patches of alder shrubland in an altitudinal band within the upper backslope; it
147 should be emphasized that Teller lacks tussock-lichen tundra and alder (*Alnus viridis* ssp. *fruticosa*) shrubs that are a

Formatted: Superscript

Formatted: Superscript

148 feature of Kougarak. While continuous permafrost largely remains, the Kougarak site appears to be undergoing
149 environmental changes as evidenced by an increase in alder coverage over the past decades (Salmon et al., 2019). Soil
150 profiles underneath the alder patches are rocky with shallow bedrock and warmer permafrost (**Table 2**). Shrub tundra
151 (alder savanna in tussock tundra and willow-birch tundra) dominates the lower backslope, where the annual active
152 layer thickness is typically less than 100 cm. Vegetation type, moisture content, permafrost extent, and hillslope
153 position at all Kougarak stations are summarized in **Table 2**.

154 2.2 Sampling & Analytical Approach

155 SPWs were sampled using two complimentary techniques. Fiberglass wicks (Frisbee [et al.](#), [Phillips, Campbell, and](#)
156 [Hendriekx](#), 2010) were deployed in the upper 30 cm of soils at stations where shallow soils were unsaturated. These
157 wicks were left in place from year-to-year and only replaced if damage was observed or suspected. The sample
158 reservoirs from the wicks were collected whenever possible, usually a few times each summer. MacroRhizons
159 (Rhizosphere Research Products; Netherlands) were used at stations that were more saturated, also targeting the upper
160 30 cm of soils. Both techniques were used at stations of intermediate saturation, where both could be deployed
161 effectively. MacroRhizons represent a relatively discrete temporal sampling event (minutes to hours), whereas wicks
162 represent a cumulative water collected over longer periods (weeks to months). It is in this sense, that the two techniques
163 are complimentary. Unfortunately, due to saturation variability both techniques could not be used at all stations and
164 conditions at some Kougarak stations were sometimes too dry to collect meaningful volumes of SPW using either
165 method. Additional SPW data from Kougarak were supplemented from a separate study focused on alder-related
166 nutrient dynamics (McCaully et al., [2022In-Review](#)). These data were collected by MacroRhizons and are captured
167 as Kougarak Stations 10 – 13, which were not part of the original stations established by the NGEE Arctic Program.
168 A total of 309 SPW samples from Kougarak were collected and analysed, whereas a total of 89 SPW samples from
169 Teller were collected and analysed.

170 After collection, SPW cation concentrations were measured in triplicate by inductively coupled plasma optical
171 emission spectroscopy (Optima 2100 DV; PerkinElmer, USA) following US EPA Method 200.7. Inorganic anion
172 concentrations were measured by ion chromatography (DX-600; Dionex, USA) following US EPA Method 300.0. B,
173 F, K, Na, and Si concentrations collected by wicks were excluded from the dataset due to known issues with these
174 ions leeching from fiberglass wick samplers (Perdrial et al., 2014; Wallenberger and Bingham, 2009). This effect is
175 illustrated in [Supplementary Figure 1](#) and the lack of such an effect for divalent cations is shown in [Supplementary](#)
176 [Figure 2](#). Comparison of data from wicks and MacroRhizons, along with the observations from (Perdrial et al., 2014),
177 demonstrates that remaining constituents discussed herein were not affected by collection with fiberglass wicks.
178 Alkalinity, pH, and E_H are all critical geochemical parameters that are susceptible to change during storage (Petron
179 [et al.](#), [Hinzman, Shibata, Jones, and Boone](#), 2007); because of the large amount of data from wicks these parameters
180 were not considered further, except in the context of thermodynamic modelling.

181 Observations related to vegetation, soil moisture, and permafrost extend were compiled from datasets made available
182 by the NGEE Arctic project and are given for Teller in **Table 1** and for Kougarak in **Table 2**. The reported soil
183 moisture contents were derived from an average of gravimetric measurements (2017 and 2018) and time domain

Formatted: Font: Bold

Formatted: Font: Bold

184 reflectometry measurements (2017 and 2019), and from remotely-sensed P-band Synthetic Aperture Radar (2017).
185 End-of-winter snow depths were measured in March and April of 2016, 2017, and 2018. The annual average ground
186 temperature was measured using in-situ temperature sensors (HOBO U30 DataLogger) at a depth of 1.5 meters below
187 the ground surface (Romanovsky et al., 2020a; Romanovsky, Cable, and Dolgikh, 2020b) and the active layer
188 thicknesses were determined by frost probe in September 2019 at the end of the growing season. Vegetation data were
189 collected at the peak of the growing season in mid to late July 2016 and 2017 at the NGEE Arctic Kougarok and Teller
190 field sites, respectively. The distribution of plant communities in the Arctic is primarily controlled by landscape,
191 topography, soil chemistry, soil moisture, and the plants that historically colonized an area (Raynolds et al., 2019).
192 Soil available rooting depth, which can be limited by shallow depths to bedrock, permafrost, or the water table, can
193 also restrict plant growth and survival of certain species by reducing access to water and nutrients. We surveyed the
194 dominant plant communities along each hillslope, which varied in their shrub abundance, canopy height, and structure,
195 to characterize the vegetation composition at the sites following the recommended protocol of Walker et al. (2016).
196 Extensive field site details and vegetation sampling methods are more thoroughly described in previous studies
197 (Salmon et al., 2019; Langford et al., 2019; Yang et al., 2020; Sulman et al., 2021; Yang et al. 2021).
198 For this study, we provide summary statistics for vegetation plots associated with intensive stations. Vegetation
199 composition plots within each intensive station were chosen subjectively in areas of homogeneous and representative
200 vegetation varying in size from 1 to 25 m² depending on canopy structure and height. The surveyed plot area was 1 ×
201 1 m for all plant communities except for the taller stature willow-birch tundra, mesic willow shrubland (2.5 × 2.5 m),
202 and alder shrubland (5 × 5 m). For each plot, all plant species (vascular plants, lichens, and bryophytes) were recorded
203 along with visual estimates of their percent cover. For plots with multiple canopies, field cover estimates were recorded
204 as absolute cover, meaning that the total cover per plot can be >100%. We calculated relative cover values (adding to
205 100%) from the field data and use these for all subsequent analyses.
206 Plant species were further aggregated into nine plant functional types (PFTs), groupings of plant species that share
207 similar growth forms and roles in ecosystem function (Wullschleger et al., 2014), based on growth patterns and plant
208 traits. PFTs in this study include: (1) nonvascular mosses and lichens, (2) deciduous and evergreen shrubs of various
209 height classes, including an alder PFT, (3) graminoids, and (4) forbs. Photos of representative PFTs from both sites
210 are given in **Supplementary Figures 9-17**. Canopy height was estimated within each plot for each PFT as the average
211 of 4 measurements, including a maximum canopy height. Active layer depth was measured at the end of the growing
212 season for all plots in September 2018 using a frost probe. A temperature probe was used to determine if the resistive
213 layer was permafrost (<0 °C) or rock (>2 °C). Thaw depth is an average of 4 measurements from the vegetation plot
214 corners.

Formatted: Superscript

Formatted: Font: Bold

215 2.3 Statistical Analysis

216 Principal Components Analysis (PCA) and the Mann-Whitney U-Test (MWUT) were both used to investigate
217 dominant environmental controls on solute concentrations in SPWs at Teller and Kougarok. PCA is an exploratory
218 data analysis tool that reduces the dimensionality of large complex datasets and considers how components (i.e. solute
219 concentrations) vary together. Because PCA was predominately used as a screening tool to reveal geochemical

220 correlations that may not have been evident by traditional geochemical causations or inference, a detailed discussion
221 of the PCA results is reserved to the Supplementary Materials. The MWUT was used to test for significant differences
222 in solute concentrations between Teller and Kougarok (inter-site variability) and between stations at each site (intra-
223 site variability). The MWUT is a non-parametric method of challenging a null hypothesis, which in this case is the
224 assumption that the concentrations of a given solute are not systematically greater at either site nor at any particular
225 station. Water chemistry data are typically not normally distributed and thus, non-parametric difference tests such as
226 the MWUT are preferred. The MWUT challenges the distribution of values, not the means. In this work, the level of
227 significance associated with the null hypothesis was operationally defined as 0.05, which equates to a 95 % chance
228 that an observed statistical difference is real and not coincidental. This error rate is operationally defined per contrast
229 (i.e. a 95 % chance that the observed statistical difference in nitrate concentrations between Teller Station 9 and Teller
230 Station 7 is real or that the observed statistical difference in sulphate concentrations between Teller and Kougarok is
231 real) as opposed to familywise (i.e. a 95 % chance that all of the observed/reported statistical differences are real and
232 not coincidental). MWUTs were completed using the methods described in Corder and Foreman (2009) and PCA was
233 completed using packages available in R statistical software, version 3.3.6 (Corder and Foreman, 2009; R Core Team,
234 2020). For all analyses, concentrations below the method detection limit were operationally defined as half the
235 detection limit, in agreeance with (Helsel, 2005, p. 43). While the emphasis of this study was on site/station (i.e.
236 spatial) variability, it should be recognized that seasonal and inter-annual variability could also be significant. To
237 minimize seasonal forcing on the variability observed, all SPW geochemical data presented were collected during the
238 thaw season between June and September.

239 **2.4 Thermodynamic Modelling**

240 To investigate thermodynamic controls on solute behaviour, particularly solubility limitations, thermodynamic
241 modelling exercises were undertaken using PHREEQC, a thermodynamic geochemical modelling code, and
242 PhreePlot, which facilitates repetitive PHREEQC calculations through looping (Kinniburgh and Cooper, 2011;
243 Parkhurst and Appelo, 2013). Because this study was focused on elucidating the primary geochemical controls on
244 solute concentrations in SPWs and not on developing a rigorous transport model, representative concentrations were
245 used instead of station specific concentrations. Representative “low”, “median”, and “high” concentration conditions
246 were proxied from the 25th, 50th, and 100th concentration percentiles, respectively, taken from both Teller and
247 Kougarok (Supplementary **Table 4**). Meanwhile, representative pH and E_H ranges were determined either through
248 direct measurement (pH), or indirectly by correlating dissolved Fe^{2+} concentrations and pH with a redox condition
249 through geochemical models and the Nernst equation. Modelling exercises were performed at 25 °C—utilizing the
250 phreeqc.dat database, with the only modification being the suppression of methane production by inorganic carbonate
251 reduction. Modelling exercises were performed at the default PHREEQC modelling temperature (25 °C), as the
252 selection of an alternative defensible temperature was non-trivial: temperatures on the Seward Peninsula span a very
253 wide range and its unclear what temperature would be most suitable for mineral solubility limitation modelling.
254 Ultimately, because the thermodynamic models were used as a tool understand what could be controlling soil pore
255 water solute concentrations and were not intended to model the system or to predict future concentrations, the default

256 temperature was decided to be the most suitable. While there is some temperature dependence of mineral solubility,
257 the differences in predicted solubility between 4 °C and 25 °C did not impact the interpretation of our results
258 (Supplementary Figure 8). Methane production was “turned-off” to maintain carbonate availability under reducing
259 conditions to help identify any possible carbonate minerals that could be precipitating. Because alkalinity was only
260 measured in a small number of samples, carbonate concentration percentiles were estimated from charge imbalances.
261 Alkalinity and charge imbalance were very well correlated in samples where alkalinity was measured
262 (Supplementary Figure 3). Although not a particularly rigorous modelling exercise, this approach was sufficient to
263 identify mineral phases that could be controlling solute generation processes through solubility limitations.

Formatted: Font: Bold

Formatted: Font: Bold

264 3. Results

265 3.1 Physical Characteristics of Stations (Co-Located Studies)

266 Controls on the observed spatial variability of SWP solute concentrations at Teller and Kougarok stations were
267 deduced, in part, from differences in physical features and conditions of each station. Quantitative measures of many
268 of these physical characteristics were available from the interdisciplinary studies co-located at the Teller and Kougarok
269 stations. The extent of permafrost, ground temperature, active layer depth, soil moisture content, snow depth,
270 vegetation type, vegetation canopy height, dominant plant functional type, and hillslope position were all compiled
271 from these co-located studies. Using these measures, the physical characteristics of each station are summarized in
272 Table 1 and Table 2, grouped by vegetation type.

273 3.1.2 Inter-site Variability: Teller versus Kougarok

274 Mann-Whitney U-Testing revealed that the concentrations of 14 of the 23 constituents analysed were significantly
275 different ($1.96 < |z|$) between Teller and Kougarok (Table 3). The effect size, a measure of how significantly different
276 the concentrations were, were large for Na and F; medium-large for K and Si; medium for Al, Oxalate, B, Zn, $\text{SO}_4\text{SO}_4^{2-}$
277 , Fe, Ba, Ti, and NO_3^- ; and small-medium for Li. The terminology and thresholds for these semi-quantitative
278 differences in correlation were taken from Corder and Foreman (2009). Mann-Whitney U-testing revealed that SPW
279 concentrations of many constituents were significantly different between Teller and Kougarok (Table 3). When
280 concentrations were significantly different between the sites, Kougarok generally exhibited the higher concentrations
281 of the two. SPW concentrations of Na, F, K, Si, Al, oxalate, B, Zn, Fe, Ba, Ti, NO_2 , and Li were all significantly
282 greater at Kougarok than Teller, while only SO_4^{2-} concentrations were significantly greater at Teller. Meanwhile, the
283 concentrations of Br, NO_3^- , Sr, PO_4 , Mg, Cr, Mn, Cl, and Ca were not significantly different between Teller and
284 Kougarok. When concentrations were significantly different between the sites, Kougarok generally exhibited the
285 higher concentrations of the two. Only SO_4 concentrations were significantly greater at Teller. The concentrations of
286 Br, NO_3 , Sr, PO_4 , Mg, Cr, Mn, Cl and Ca were not significantly different between Teller and Kougarok. A summary
287 of the inter-site MWUT results are given in Table 3 with the constituents that exhibited significant differences between
288 the sites displayed over a darkened background.

Formatted: Subscript

Formatted: Superscript

289 **3.2.3 Intra-site Variability: Teller and Kougarok Stations**

290 Mann-Whitney U-Testing was also used to test for intra-site differences between stations at both Teller and Kougarok.
291 Boxplots and compact letter displays are used to visualize the within-site variability of a select group of constituents
292 of interest (COIs), which are given in **Figure 4**. Tables of the results of the intra-site MWUTs for all constituents that
293 were monitored, including those that did not demonstrate some systematic inter-station variability or were not
294 otherwise of interest, are given in the Supplementary Materials.

295 **3.3 Physical Characteristics of Stations (Co-Located Studies)**

296 Controls on the observed spatial variability of SPW solute concentrations at Teller and Kougarok stations were
297 deduced, in part, from differences in physical features and conditions of each station. Quantitative measures of many
298 of these physical characteristics were available from the interdisciplinary studies co-located at the Teller and Kougarok
299 stations. The extent of permafrost, ground temperature, active layer depth, soil moisture content, snow depth,
300 vegetation type, vegetation canopy height, dominant plant functional type, and hillslope position were all compiled
301 from these co-located studies. Using these measures, the physical characteristics of each station are summarized in
302 **Table 1** and **Table 2**, grouped by vegetation type.

303 **4. Discussion**

304 **4.1 Inter-site Variability: Teller versus Kougarok**

305 Mann-Whitney U testing revealed that SPW concentrations of many constituents were significantly different between
306 Teller and Kougarok (**Table 3**). SPW concentrations of Na, F, K, Si, Al, oxalate, B, Zn, Fe, Ba, Ti, NO₂, and Li were
307 all significantly greater at Kougarok than Teller, while only SO₄ concentrations were significantly greater at Teller.
308 Meanwhile, the concentrations of Br, NO₃, Sr, PO₄, Mg, Cr, Mn, Cl, and Ca were not significantly different between
309 the two sites. Overall, the more frequent instance of significantly greater constituent concentrations at Kougarok
310 suggests a systematic cause. The extensive low gradient toeslope (**Figure 2**) and lack of a well defined drainage
311 channel at Kougarok, are likely causes of the systematically higher SPW solute concentrations at Kougarok. Water
312 perching, the result of near surface permafrost in the lower backslope and toeslope, increases evapotranspiration and,
313 thus, SPW solute concentrations. Meanwhile, the lack of a drainage channel at Kougarok suggests that runoff (and
314 therefore solute exports) is more limited than at Teller. Without a relatively rapid export mechanism such as a stream
315 channel, solute transport is likely limited to interflow within the Kougarok hillslope over much of the thaw season,
316 allowing weathering products to increase to significantly greater concentrations than those observed at Teller, where
317 a well defined drainage/export mechanism does exist. Field observations from pits at Kougarok confirm the present
318 of interflow at the site. The exception to the general observation of elevated concentrations at Kougarok versus Teller
319 was SO₄. Although the cause of consistently higher SO₄ concentrations at Teller is unclear from the limited scope of
320 this study, it seems likely to be due to a greater abundance of sulfidic bedrock material. The presence of sulfidic
321 bedrock in the vicinity of Teller has been reported by mineral prospecting efforts (Brobst, Pinckney, and Sainsbury,
322 1971; Herreid, 1966; Mulligan, 1965); we are unaware of any such reports near Kougarok.

4.2 Intra-site Variability: Teller and Kougarok Stations

Our interpretation of the major environmental controls on the observed spatial variability of SPW solute concentrations between stations are shown in Table 4. Each of these controls, including vegetation effects, soil moisture and redox effects, weathering, water/soil interactions and hydrological transport effects, and mineral solubility effects, is discussed-considered in detail in the following sections.

3.4.3.1 Vegetation Effects

Vegetation can influence hydrogeochemical variability directly via vegetation-induced changes to elemental cycling and soil moisture contents, or indirectly via the secondary impacts changes in soil moisture can have on mineral solubility or on the soil redox condition. The geochemical consequences of solubility and redox conditions are the focus of sections to follow, thus, this section will focus on direct vegetation effects via influences on elemental cycling and soil moisture via evapotranspiration and preferential trapping of snow.

NO_2NO_3^- was the only COI that showed a distinct effect from vegetation via elemental cycling.- Elevated NO_2NO_3^- concentrations were associated with the presence of alder shrubs and, in some cases, willow shrubs. NO_2NO_3^- concentrations at both sites were generally low, with the exception of Kougarok Stations 3, 5, and 12, and Teller Station 7 (Figure 4). **Low to tall alder shrubs are the dominant vegetation type at Kougarok Stations 3 and 12 (Table 2).** Meanwhile, alders are present at Kougarok Station 5 despite the dominant vegetation type being low willow and birch shrubs. Kougarok Stations 3, 5, and 12 all have a significant alder presence. Alders increase soil nitrogen through a symbiotic relationship with nitrogen-fixing bacteria that reside in their root nodules, thus, an association between NO_2NO_3^- concentrations and alder vegetation is expected (Salmon et al., 2019).

Perhaps more noteworthy was ~~the elevated NO_2 at Kougarok Station 5 and~~ the lack of elevated NO_2NO_3^- concentrations at Kougarok Stations 1, 2, 6, 10, and 11. The vegetation type at Kougarok Stations 1, 2, 6, 10, and 11 is alder savanna in tussock tundra, which is a mixed graminoid-shrub tundra with shorter stature and lower density of alder shrubs, yet nonetheless nitrogen input via alder derived nitrogen-fixation is anticipated to occur. The lack of elevated NO_2NO_3^- suggests either that 1) nitrogen-fixation in alder savanna in tussock tundra is insufficient to result in an increase in NO_2NO_3^- concentrations, 2) that the Kougarok footslope and lower backslope is very nitrogen-limited, and thus, that NO_2NO_3^- is largely consumed by vegetation as it is fixed, or 3) that microbes in the Kougarok footslope and lower backslope rapidly denitrify the available NO_2NO_3^- as a substitute for oxygen in their metabolisms. The smaller shrub size and density in the alder savanna in tussock tundra certainly results in less accumulated leaf litter relative to the denser and larger alder shrubland intensive stations, as such, it seems reasonable that less nitrogen would be available at stations in alder savanna in tussock tundra. Meanwhile, isotopic measurements of nitrogen downslope of alder patches at Kougarok Stations 12 and 3 also support the occurrence of denitrification (McCaully et al., *In Review*2022). Therefore, we believe the lack of elevated NO_2NO_3^- concentrations at Kougarok Stations 1, 2, 6, 10, and 11 is a combination of less alder leaf litter and greater denitrification, than at Kougarok Stations 3, 5, or 12.

At Teller, only Station 7 exhibited elevated NO_2NO_3^- concentrations relative to the rest of the catchment (Figure 4). Teller Station 7 is dominated by tall willow shrubs and is relatively dry. Mineralization and nitrification of willow leaf litter coupled with limited microbial denitrification is the presumed cause of elevated NO_2NO_3^- concentrations at

Formatted: Heading 2,Sub_Heading

Formatted: Subscript

Formatted: Subscript

Formatted: Subscript

Formatted: Font: Bold

Formatted: Not Superscript/ Subscript

Formatted: Not Superscript/ Subscript

Formatted: Superscript

359 Teller Station 7. Teller Station 2 also has tall willow shrubs but did not exhibit elevated NO_3NO_3^- concentrations.
360 From the limited scope of this study, it is unclear why Teller Station 2 did not exhibit elevated NO_3NO_3^- while Station
361 7 did, but we suspect that higher seasonal moisture content and greater microbial denitrification at Teller Station 2
362 likely played a role. Also of note was that despite significant intra-site NO_3NO_3^- concentration differences, inter-site
363 differences were not significant ($|z| = 1.59$) and that relatively few Kougarak stations showed elevated NO_3NO_3^-
364 concentrations, despite a widespread alder presence. Increased microbial denitrification is suspected to balance
365 increased nitrogen-fixation at these stations. This is consistent with previous studies that have noted higher nitrogen
366 mineralization rates in acidic tundra than non-acidic tundra (Weiss et al., 2005); Kougarak is predominantly acidic
367 tundra and Teller is non-acidic tundra.

368 The effect of vegetation on spatial variability of soil moisture was not readily observed in the volumetric moisture
369 content of soil (Table 1 and Table 2) but was somewhat apparent in the spatial variability of moisture sensitive
370 constituents, such as Cl (Figure 4). The lack of a clear correlation between vegetation and soil moisture by TDR or
371 P-band SAR observations is perhaps due to the coarseness of the P-band SAR observations and the strong seasonality
372 associated with both methods. Moisture sensitive constituents, such as Cl, may provide a more seasonally averaged
373 tracer of soil moisture content at the stations. An increase in Cl concentrations with vegetation canopy height was
374 apparent at Teller stations suggesting an evapotranspiration effect. This trend was also apparent at Kougarak, but the
375 differences were rarely significant. Overall, the spatial variability of soil moisture sensitive constituents, like Cl, was
376 far less correlated with vegetation-type than expected; perhaps due to preferential trapping of snow, which may offset
377 the increased evapotranspiration of tall shrubs more than previously realized. Overall, Cl concentrations at Kougarak
378 appeared to be more correlated with hillslope position than with vegetation canopy height (Figure 4).

379 3.3.2.4.4 Soil Moisture and Redox Effects

380 Soil moisture content can have a profound effect on redox sensitive elements. Saturation limits oxygen diffusion into
381 soil, and thus, forces microorganisms to utilize less energetic electron acceptors to metabolize organic matter. In an
382 ideal system, soil microorganisms will use the strongest electron acceptor available, until it is exhausted. Although
383 natural environments are not ideal systems, redox conditions in soils follow a more or less stepwise progression.
384 Therefore, by evaluating the dissolved concentrations of NO_3NO_3^- , Mn, Fe, and $\text{SO}_4\text{SO}_4^{2-}$ in SPWs, it is possible to
385 qualitatively assess soil redox conditions and their impact on hydrogeochemical variability.

386 The redox conditions at both Teller and Kougarak are generally limited by Fe reduction, with the most reducing
387 conditions found at stations with the highest soil moisture content. As such, NO_3NO_3^- concentrations are generally
388 low (Table 3), $\text{SO}_4\text{SO}_4^{2-}$ concentrations are relatively consistent (Figure 4), and Mn and Fe concentrations increase
389 with increasing soil moisture (Figure 4). NO_3NO_3^- concentrations were generally low, except for drier stations in the
390 proximity of tall alders or willows. While NO_3NO_3^- inputs are discussed in the vegetation effects section, the lack of
391 high NO_3NO_3^- concentrations at wetter stations that contain alders suggests that soil moisture coupled with microbial
392 denitrification exerts a strong control on SPW NO_3NO_3^- concentrations. Meanwhile, $\text{SO}_4\text{SO}_4^{2-}$ concentrations at both
393 sites are relatively constant across clear moisture and redox gradients (Figure 4). This suggests that $\text{SO}_4\text{SO}_4^{2-}$
394 reduction is not pervasive at either site. Dissolved Fe concentrations were higher at stations with higher soil moisture

Formatted: Not Superscript/ Subscript

Formatted: Superscript

395 content, consistent with Fe reduction. Similarly, Mn concentrations were slightly elevated at wetter stations. The
396 concentrations of Mn, however, rarely rose above 0.05 mg·L⁻¹, suggesting either Mn solubility limitations or a lack
397 of a significant Mn weathering source. Low Mn concentrations at Teller Station 5, a wetter station on the upper
398 shoulder of the Teller watershed (**Table 1; Figure 2**) seems to support the latter conclusion, as do geochemical
399 modelling exercises (Section 4.5). Together, these results suggest that the most reducing condition at both sites is
400 typically limited to Fe reduction and that this only occurs at stations with the highest soil moisture contents.

401 **4.43.3.3 Weathering, Water/Soil Interaction, and Hydrological Transport Effects**

402 A combination of weathering, water/soil interactions, and hydrological transport were ~~clear-identified as probable~~
403 drivers of hydrogeochemical variability for some solutes. As noted by Philben et al. (2020), soil derived solutes tend
404 to accumulate in low-lying areas within watersheds. This is ~~clearly-seenobserved~~ at Teller, where the concentrations
405 of Ca, Sr, and Mg all increase dramatically at the transition from lower backslope to footslope (**Figure 5**). Both Teller
406 and Kougarok are underlain by carbonate-rich metamorphic facies, and Ca, Sr, and Mg are probable carbonate counter-
407 cations. Weathering of Ca, Sr, and Mg carbonates and subsequent transport of these cations downslope explains this
408 pattern of spatial variability. At Kougarok, concentrations of Ca, Mg, and Sr similarly increase from upper backslope
409 to footslope, but concentrations of Ca and Sr decrease further down the lower backslope (Stations 10 and 1), while
410 Mg concentrations continue to increase. A possible explanation for this behaviour is the greater affinity of cation
411 exchange surfaces for Ca and Sr compared to Mg, thus, Ca and Sr are preferentially retained in the footslope whilst
412 Mg is transported further down the lower backslope (Sparks, 2003, p. 189).

413 **4.53.3.4 Mineral Solubility Effects**

414 Although redox reactions are rarely at equilibrium in natural environments, comparison of field data with equilibrium
415 models provides valuable semi-quantitative insight into the redox condition of natural environments. Because Fe
416 appeared to be limiting the development of more reducing conditions (Section 4.3), select samples from both sites
417 were measured for soluble Fe²⁺ following methods presented in Viollier et al. (2000). These concentrations of aqueous
418 Fe²⁺ were then compared with model-predicted concentrations of Fe²⁺, when coupled with an infinite Fe(OH)_{3(am)}
419 phase, across a range of pH values (2 – 10) and fixed E_H values of 400 mV, 200 mV, 0 mV, and -200 mV; activity
420 coefficients were assumed to be equal to 1. The measured and modelled Fe²⁺ concentrations are compared in **Figure**
421 **6**, where concentrations that were below the method detection limit (0.05 mg·L⁻¹) are set equal to 0.025 mg·L⁻¹ (half
422 the detection limit). Comparison of model predicted Fe²⁺ concentrations with field data suggests that while Teller
423 exhibits a narrower range of pH conditions than Kougarok, it exhibits a broader range of redox conditions (**Figure 6**).
424 Although several Fe²⁺ measurements were below the detection limit, suggesting oxidizing conditions, high Fe²⁺
425 concentrations in some samples suggested E_H values below 0 mV. Therefore, Fe redox conditions at Teller ranged
426 from mildly reducing to oxic and Fe redox conditions at Kougarok ranged from mildly oxic to oxic. Oxidation-
427 reduction potentials (ORPs), calculated from pH, Fe²⁺ concentrations, and the Nernst equation suggest that ORPs at
428 Teller were as low as -69 mV, while the lowest ORP at Kougarok was +134 mV (**Figure 6**). Maximum ORP values
429 could not be determined quantitatively as some Fe²⁺ concentrations were below Fe²⁺ detection limits, at both sites.

430 E_H/pH predominance diagrams were created from the 25th, 50th, and 100th concentration percentiles and are shown
431 in **Figure 7** for the COIs where precipitation of mineral phases were predicted under some conditions. The
432 concentrations for these diagrams were taken from filtered aqueous concentration data, thus, predicted mineral
433 precipitation is an indication of nearly saturated or over-saturated conditions. The range of E_H and pH conditions
434 observed at Teller and Kougarok are overlaid as solid yellow and solid blue lines, respectively. Only the predominance
435 diagrams that indicated possible mineral formation under the E_H/pH conditions present at either site are shown in
436 **Figure 7**. These phases included Fe(OH)_{3(am)} (Fe), siderite (Fe), Al(OH)_{3(am)} (Al), chalcedony (Si), barite (Ba and
437 SO₄), calcite (Ca), dolomite (Ca and Mg), and rhodochrosite (Mn). Predominance diagrams for the remaining key
438 COIs that were not predicted to form any mineral phases under any site conditions are given in **Supplementary Figure**
439 **4**.

440 -To further examine which mineral phases could be controlling ~~solute generation processes~~ **SPW solute concentrations**,
441 saturated conditions for the mineral phases identified in **Figure 7** were modelled using sweeps of pH values from 2 –
442 10 at various fixed E_H values (400mV, 200mV, 0mV, and -200mV). Predicted solute concentrations under the
443 modelled saturated conditions were then compared with field data to find common trends. In general, if solute
444 concentrations were frequently measured near the saturation of a mineral, or were identified to have similar
445 dependence on pH or E_H, it was inferred that the mineral phase could be controlling the generation of that solute. The
446 mineral phases that were identified to possibly be controlling solute concentrations were Al(OH)_{3(am)}, Fe(OH)_{3(am)},
447 chalcedony, and barite. This does not preclude the presence of significant concentrations of other mineral phases, it
448 only identifies these as ~~likely possibly~~ controlling the dissolved concentrations of Al, Fe, Si, and Ba, respectively.
449 Although it does not provide mineralogical information, X-ray fluorescence (XRF) data reported by another study at
450 Teller confirmed high concentrations of Al, Fe, Si, and Ba in the organic and mineral soil layers at that site (Graham
451 et al., 2018). We are unaware of any similar studies at Kougarok, nor are we aware of any studies that provide would
452 provide confirmatory mineralogical information, for example by X-ray diffraction (XRD).

453 Aluminium concentrations in SPWs at both Teller and Kougarok appear to be controlled by the
454 dissolution/precipitation of amorphous Al hydroxide (Al(OH)_{3(am)}) (**Figure 8**). The solubility limit of Al(OH)_{3(am)} has
455 no redox dependence, but is highly pH dependent. Aluminium concentrations were generally clustered near the
456 solubility limit of Al(OH)_{3(am)}; Al(OH)_{3(am)} + 3H⁺ ↔ Al³⁺ + 3H₂O; log k = 10.8. This suggests that Al SPW
457 concentrations at both sites are controlled by wetting/drying (dissolution/precipitation) processes. It also suggests that
458 there could be a significant amount of Al(OH)_{3(am)} in the soils at both sites. While organic matter may also sorb to
459 alumina surfaces, the adherence to the solubility of Al(OH)_{3(am)} suggests that significant concentrations of Al are not
460 complexed with dissolved organic matter. The predominance diagrams highlight 1) the strong pH dependence on the
461 stability of Al(OH)_{3(am)}, 2) the influence of dissolved F can have on Al speciation when Al concentrations are low,
462 and 3) that Al is a cation at low pH and an anion at high pH (**Figure 7**). Despite being a weathering product, Al
463 concentrations show a dissimilar downslope trend to other weathering products, especially at Teller (**Supplementary**
464 **Figure 5**). While the concentrations of weathering products generally increase with distance downslope, Al
465 concentrations decrease. We suspect this can be attributed to increasing pH with distance downslope. Philben et al.
466 (2020) reported a 1 pH unit increase in pH in organic soils along the Teller transect (**Figure 2**), increasing from 5.6 at

Formatted: Font: Bold

Formatted: Font: Bold

467 Station 5 to 6.7 at Station 9. Such an increase would decrease the solubility of $\text{Al}(\text{OH})_{3(\text{am})}$, and thus, decrease the
468 concentration of dissolved Al (**Figure 8**).

469 Similar to Al, Fe concentrations in SPWs at both Teller and Kougarok appear to be controlled by the
470 dissolution/precipitation of amorphous Fe hydroxide ($\text{Fe}(\text{OH})_{3(\text{am})}$). Fe concentrations were generally clustered near
471 the solubility limit of $\text{Fe}(\text{OH})_{3(\text{am})}$ (**Figure 8**). Unlike $\text{Al}(\text{OH})_{3(\text{am})}$ however, $\text{Fe}(\text{OH})_{3(\text{am})}$ solubility is dependent on the
472 redox condition in addition to the pH; $\text{Fe}(\text{OH})_{3(\text{am})} + 3\text{H}^+ + \text{e}^- \leftrightarrow \text{Fe}^{2+} + 3\text{H}_2\text{O}$; $\log k = 16.0$ (**Figure 8**). Fe(III) is only
473 sparingly soluble in aqueous solutions and reduction to Fe(II) significantly increases the solubility of Fe, thus, at a
474 given pH value higher aqueous concentrations are predicted and observed under more reducing conditions (**Figure 8**).
475 Iron concentrations in SPWs at both sites generally follow the pH dependence of $\text{Fe}(\text{OH})_{3(\text{am})}$ solubility (**Figure 8**).
476 This suggests that SPW concentrations of Fe at both sites are controlled by wetting/drying (dissolution/precipitation)
477 processes, coupled with the redox condition.

478 Si concentrations are frequently limited by the solubility of chalcedony (**Figure 8**), a very finely grained form of SiO_2 ,
479 which is much more soluble than quartz; $\text{SiO}_2 + 2\text{H}_2\text{O} \leftrightarrow \text{H}_4\text{SiO}_4$; $\log k = -3.55$. Particularly at Kougarok, the
480 dissolved Si concentrations, coupled with a lack of a strong pH or E_{H} dependence, suggest a controlling influence of
481 chalcedony (**Figure 8**).

482 Ba concentrations also appear to be controlled by solubility, but rather than by the solubility of an oxide or a hydroxide
483 phase, by the solubility of barite (**Figure 8**) [$\text{Ba}^{2+} + \text{SO}_4^{2-} \leftrightarrow \text{BaSO}_4(\text{s})$; $\log k = 9.97$]. Unlike Al hydroxide or Fe
484 hydroxide, barite solubility lacks a strong pH dependence and instead is dependent solely on the activities of Ba^{2+} and
485 SO_4^{2-} . Unlike Ba, $\text{SO}_4\text{SO}_4^{2-}$ concentrations are not limited by the solubility limit of barite and are generally higher and
486 not well correlated with Ba concentrations. Together, these suggest that $\text{SO}_4\text{SO}_4^{2-}$ from another source (likely,
487 atmospheric deposition or sulfidic mineral oxidation), is suppressing barite dissolution, and thus, is reducing dissolved
488 Ba concentrations. Barite solubility can exhibit a redox dependence if conditions are sufficiently reducing to reduce
489 $\text{SO}_4\text{SO}_4^{2-}$ to sulphide (Neff, 2002). This shifts the equilibrium to greater dissolution of barite, and therefore higher
490 conditions of Ba. The lack of E_{H} dependence in observational data further suggests that neither site exhibits significant
491 $\text{SO}_4\text{SO}_4^{2-}$ reduction.

492 **54. ConclusionsDiscussion**

493 The 18 stations examined herein (8 at Teller and 10 at Kougarok) represent a wide range of vegetation types, soil
494 moisture contents, permafrost extents, and hillslope positions. Coupling the spatial variability of these landscape
495 characteristics with the spatial variability of SPW solute concentrations provides valuable insight into the dominant
496 environmental controls on observed spatial variability of SPW geochemistry. It is our hope that correlating SPW
497 geochemistry with readily observable and scalable landscape features will inform earth system modelling efforts in
498 permafrost regions and provide fast and easy methods to determine if earth system models are working properly (i.e.
499 predicting the correct trends). The inferred dominant environmental controls on the observed inter-site and intra-site
500 variability of SPW solute concentrations are discussion in the following sections.

Formatted: Font: Bold

Formatted: Subscript

501 **4.1 The Dominant Environmental Controls on Inter-site Variability of SPW Solute Concentrations**

502 Overall, the more frequent instance of significantly greater constituent concentrations at Kougarok suggests a
503 systematic cause. The extensive low-gradient toeslope (Figure 2) and lack of a well-defined drainage channel at
504 Kougarok, are likely causes of the systematically higher SPW solute concentrations at Kougarok. Water perching, the
505 result of near-surface permafrost in the lower-backslope and toeslope, is likely to increase evapotranspiration and,
506 thus, SPW solute concentrations. Significant evapotranspiration caused by supra-permafrost water table perching has
507 been noted in several previous studies (Huang et al., 2022; Park et al., 2021; Sjöberg et al., 2021). Meanwhile, the
508 lack of a drainage channel at Kougarok suggests that runoff (and therefore solute exports) is more limited than at
509 Teller. Without a relatively rapid export mechanism such as a stream channel, solute transport is likely limited to
510 interflow within the Kougarok hillslope over much of the thaw season, allowing weathering products to increase to
511 significantly greater concentrations than those observed at Teller, where a well-defined drainage/export mechanism
512 does exist. Field observations from pits at Kougarok confirm observable interflow at the site. Overall, our study
513 suggests that evaporative concentration could be a significant control on SPW solute concentrations in permafrost
514 catchments, especially in those with limited drainage and therefore a perched near-surface water table. This effect has
515 been reported previously (Raudina et al., 2017), but does not appear to be widely considered, perhaps due to the
516 generally few studies of SPW solutes in permafrost regions. We suggest future efforts to predict future SPW solute
517 and nutrient dynamics directly address the impacts of evaporative concentration on permafrost catchments, especially
518 with future permafrost thaw.

519 The exception to the general observation of elevated concentrations at Kougarok versus Teller was SO_4^{2-} . Although
520 the cause of consistently higher SO_4^{2-} concentrations at Teller is unclear from the limited scope of this study, it seems
521 likely to be due to a greater abundance of sulfidic bedrock material. The presence of sulfidic bedrock in the vicinity
522 of Teller has been reported by mineral prospecting efforts (Brobst, Pinckney, and Sainsbury, 1971; Herreid, 1966;
523 Mulligan, 1965); we are unaware of any such reports near Kougarok. It should be recognized SO_4^{2-} concentrations at
524 both Kougarok and Teller are relatively low.

Formatted: Normal

526 **4.5.12 The Dominant Environmental Controls on Intra-site Spatial Variability of SPW Solute Concentrations**

527 The 18 stations examined herein (8 at Teller and 10 at Kougarok) were selected to represent a wide range of vegetation
528 types, soil moisture contents, permafrost extents, and hillslope positions. Coupling the spatial variability of these
529 landscape characteristics with the spatial variability of SPW solute concentrations provides valuable insight into the
530 dominant environmental controls on observed spatial variability of SPW geochemistry.

531 With regard to our initial hypotheses, our major findings are that:

532 Vegetation influences on elemental cycles were only readily apparent for nitrogen and although vegetation induced
533 changes to soil moisture content were discernible, they were far less significant than anticipated. NO_3NO_2^- was the
534 only COI that exhibited a clear vegetation effect; elevated concentrations were associated with the presence of alder
535 shrubs and, in some cases, tall willow shrubs. These increases in NO_3NO_2^- concentrations associated with alder

Formatted: Subscript

Formatted: Subscript

536 nitrogen-fixation and the mineralization and nitrification of willow leaf litter were frequently equipoised by increased
537 microbial denitrification in regions sufficiently moist to support it, this is perhaps one of the most significant findings
538 of this work. –Although both Kougarok and Teller exhibited some indications of increased Cl concentrations in the
539 presence of tall shrubs, the net vegetation effect on soil moisture was far less than hypothesized. Redox sensitivity
540 was also less than ~~hypothesized~~hypothesized, and most stations seemed well-buffered at Fe redox conditions. The
541 result of this buffering was generally low NO_2NO_3^- concentrations (except where vegetation effects dominated),
542 consistent $\text{SO}_4\text{SO}_4^{2-}$ concentrations across clear redox gradients, and variable Mn and Fe concentrations. Mn
543 concentrations were generally low, likely due to a limited source. Fe concentrations were higher at stations with higher
544 soil moisture content, consistent with Fe reduction. Similar Fe redox cycling between soluble Fe(II) species and
545 precipitated Fe oxyhydroxides in permafrost catchments has been reported recently (Patzner et al., 2022), which
546 suggests that Fe redox buffering in permafrost landscapes is widespread. Weathering, water/soil interactions, and
547 hydrological transport were ~~clear~~probable drivers of variability for Ca, Sr, and Mg. Ca, Sr, and Mg all tended to
548 accumulate in low-lying areas, although Ca and Sr demonstrated greater accumulation potential than Mg, likely via
549 greater affinity of cation exchange surfaces for Ca and Sr compared to Mg. Mineral solubility limitations were the
550 primary controls on Al ($\text{Al}(\text{OH})_{3(\text{am})}$), Fe ($\text{Fe}(\text{OH})_{3(\text{am})}$), Ba (barite), and Si (chalcedony) concentrations. This suggests
551 that the SPW concentrations of these constituents will remain stable until those mineral phases are exhausted or soil
552 pore hydrochemistry changes sufficiently to alter the solubility of those mineral phases. Supersaturation of Al with
553 respect to gibbsite (crystalline $\text{Al}(\text{OH})_3$) and Si with respect to chalcedony in a permafrost wetland has been reported
554 previously (Jesson et al., 2014). The solubility curves for gibbsite and $\text{Al}(\text{OH})_{3(\text{am})}$ are similar, with $\text{Al}(\text{OH})_{3(\text{am})}$ being
555 slightly more soluble at all pH values due to the increased thermodynamic stability of the crystalline Al hydroxide
556 mineral, gibbsite. Meanwhile, seasonal precipitation of Fe oxyhydroxides in permafrost peatlands and their effect of
557 carbon cycling was the subject of an excellent paper by Patzner et al. (2022). Our study is the first observation we are
558 aware of that reports the saturation controls of barite on Ba in permafrost SPWs, although that could be because
559 relatively few studies consider barium concentrations; it is worthwhile emphasizing that Ba was not supersaturated
560 with respect to barite but approached a saturated condition. Future studies should also note that Cchanges in redox
561 condition would significantly alter $\text{Fe}(\text{OH})_{3(\text{am})}$ solubility, whereas changes in pH conditions would significantly alter
562 $\text{Al}(\text{OH})_{3(\text{am})}$ and $\text{Fe}(\text{OH})_{3(\text{am})}$ solubility.

563 Although discerning the environmental controls on spatial variability of SPW solute concentrations provides some
564 high-level insight into the effects changes in landscape character may have on soil pore hydrochemistry, our scope
565 was limited and leveraged on previously available datasets. We hope that the observations and trends discussed here
566 aid future studies in the selection of appropriate sample sites and sampling schemes. Future studies should more fully
567 consider the role of spatial variability of a catchment's solid phases (i.e. soils, leaf litter, and underlying geology). Soil
568 digestions (elemental composition), sequential extractions (organic character), or XRD (mineralogical character) all
569 would have been helpful in our work. Detailed geophysical surveys would have greatly aided our interpretation and
570 increased the significance and impact of the work. More regular sampling of soil pore waters to capture the seasonality
571 of active layer thaw, leaf fall/litter degradation, also would have provided additional insight. For catchments with
572 well-defined drainages, gauging stations with periodic sampling could also be very useful in interpretation (i.e. through

Formatted: Subscript

Formatted: Subscript

573 [concentration-discharge relationships](#)). Overall, ~~T~~he significance of SPW in small Arctic headwater catchments as a
574 key initial component in the freshwater hydrologic continuum is under recognized, and such catchments warrant more
575 detailed and systematic investigations.

576

577 **56. Acknowledgements**

578 We would like to thank the Sitnasuak Native Corporation and the Mary's Igloo Native Corporation for their guidance
579 and for allowing us to conduct this research on the traditional homelands of the Inupiat people. Funding was provided
580 by the Next-Generation Ecosystem Experiments (NGEE Arctic) project, supported by the Office of Biological and
581 Environmental Research in the U.S. DOE Office of Science. We wish to thank Lauren Charsley-Groffman and Nathan
582 Wales for their assistance with fieldwork, as well as, George Perkins, Oana Marina, Rose Harris, and Emily Kluk for
583 their assistance with laboratory analyses.

584 **76. Data availability statement**

585 The data that support the findings of this study are made openly available in the NGEE-Arctic data repository at (DOI:
586 10.5440/1735757).

587 **87. References**

588 [Anderson, M. D., Ruess, R. W., Myrold, D. D., and Taylor, D. L. \(2009\). Host species and habitat affect nodulation
589 by specific Frankia genotypes in two species of Alnus in interior Alaska. *Oecologia* 160, 619–630. doi:
590 10.1007/s00442-009-1330-0](#)

591 [Anderson, M. D., Ruess, R. W., Uliassi, D. D., and Mitchell, J. S. \(2004\). Estimating N₂ fixation in two species of
592 Alnus in interior Alaska using acetylene reduction and 15N₂ uptake. *Ecoscience* 11, 102–112. doi: 10.1080/
593 11956860.2004.11682814](#)

594 [Binkley, D., Sollins, P., Bell, R., Sachs, D., and Myrold, D.: Biogeochemistry of adjacent conifer and alder-conifer
595 stands, *Ecology*, 73, 2022–2033, 1992.](#)

596 Breen, A., Iversen, C., Salmon, V., VanderStel, H., Busey, B., and Wulfschleger, S. 2020a:. NGEE Arctic Plant Traits:
597 Plant Community Composition, Kougarak Road Mile Marker 64, Seward Peninsula, Alaska, 2016 [Data set], doi:
598 <https://doi.org/10.5440/1465967>.

599 Breen, A., Iversen, C., Salmon, V., VanderStel, H., Busey, B., and Wulfschleger, S. 2020b:. NGEE Arctic Plant Traits:
600 Plant Community Composition, Kougarak Road Mile Marker 64, Seward Peninsula, Alaska, 2016 [Data set], doi:
601 <https://doi.org/10.5440/1465967>.

602 Bring, A., Fedorova, I., Dibike, Y., Hinzman, L., Mård, J., Mernild, S. H., ... Woo, M.-K. 2016: Arctic terrestrial
603 hydrology: A synthesis of processes, regional effects, and research challenges. *Journal of Geophysical Research:*
604 *Biogeosciences*, 121: 621–649, doi: <https://doi.org/10.1002/2015JG003131>.

605 Brobst, D. A., Pinckney, D. M., and Sainsbury, C. L. 1971: Geology and Geochemistry of the Sinuk River Barite
606 Deposit, Seward Peninsula, Alaska (No. 463 (?)). United States Department of the Interior Geological Survey.

607 [Bühlmann, T., Hiltbrunner, E., and Körner, C.: *Alnus viridis* expansion contributes to excess reactive nitrogen release,
608 reduces biodiversity and constrains forest succession in the Alps, *Alpine Botany*, 124, 187–191,
609 <https://doi.org/10.1007/s00035-014-0134-y>, 2014.](#)

610 [Clein, J. S. and Schimel, J. P.: Nitrogen turnover and availability during succession from alder to poplar in Alaskan
611 taiga forests, *Soil Biology and Biochemistry*, 27, 743–752, \[https://doi.org/10.1016/0038-0717\\(94\\)00232-P\]\(https://doi.org/10.1016/0038-0717\(94\)00232-P\), 1995.](#)

612 Conroy, N., Heikoop, J., Newman, B., Wilson, C., Arendt, C., Perkins, G., and Wullschleger, S. 2021: Soil Water
613 Chemistry and Water and Nitrogen Isotopes, Teller Road Site and Kougarok Hillslope, Seward Peninsula, Alaska,
614 2016 - 2019 [Data set], doi: <https://doi.org/10.5440/1735757>.

615 Corder, G. W., and Foreman, D. I. 2009: Nonparametric statistics for non-statisticians: a step-by-step approach.
616 Hoboken, N.J.; Wiley, 247 pp.

617 Frey, K. E., and McClelland, J. W. 2009: Impacts of permafrost degradation on arctic river biogeochemistry.
618 *Hydrological Processes*, 23: 169–182, doi: <https://doi.org/10.1002/hyp.7196>.

619 Frisbee, M. D., Phillips, F. M., Campbell, A. R., and Hendrickx, J. M. H. 2010: Modified passive capillary samplers
620 for collecting samples of snowmelt infiltration for stable isotope analysis in remote, seasonally inaccessible
621 watersheds 1: laboratory evaluation. *Hydrological Processes*, 24: 825–833, doi: <https://doi.org/10.1002/hyp.7523>.

622 Fuchs, M., Nitze, I., Strauss, J., Günther, F., Wetterich, S., Kizyakov, A., ... Grosse, G. 2020: Rapid Fluvio-Thermal
623 Erosion of a Yedoma Permafrost Cliff in the Lena River Delta. *Frontiers in Earth Science*, 8: 336, doi:
624 <https://doi.org/10.3389/feart.2020.00336>.

625 Graham, D. E., Kholodov, A., Wilson, C. J., Moon, J.-W., Romanovsky, V. E., and Busey, B. 2018: Soil Physical,
626 Chemical, and Thermal Characterization, Teller Road Site, Seward Peninsula, Alaska, 2016., doi:
627 <https://doi.org/10.5440/1342956>.

628 Harms, T. K., and Jones, J. B. 2012: Thaw depth determines reaction and transport of inorganic nitrogen in valley
629 bottom permafrost soils. *Global Change Biology*, 18: 2958–2968, doi: [https://doi.org/10.1111/j.1365-
2486.2012.02731.x](https://doi.org/10.1111/j.1365-
630 2486.2012.02731.x).

631 Harms, T. K., and Ludwig, S. M. 2016: Retention and removal of nitrogen and phosphorus in saturated soils of arctic
632 hillslopes. *Biogeochemistry*, 127: 291–304, doi: <https://doi.org/10.1007/s10533-016-0181-0>.

633 Helsel, D. R. 2005: Nondetects and data analysis: statistics for censored environmental data. Hoboken, NJ.; Wiley-
634 Interscience, 250 pp.

635 Herreid, G. 1966: Preliminary geology and geochemistry of the Sinuk River area. Seward Peninsula, Alaska: Alaska
636 Division of Mines and Minerals Geologic Report, 24: 19.

637 Hiyama, T., Yang, D. and Kane, D.L., 2021. Permafrost Hydrology: Linkages and Feedbacks. In *Arctic Hydrology,
638 Permafrost and Ecosystems* (pp. 471-491). Springer, Cham.

639 [Hollingsworth, T. N., Lloyd, A. H., Nossov, D. R., Ruess, R. W., Charlton, B. A., and Kielland, K. \(2010\). Twenty-
640 five years of vegetation change along a putative successional chronosequence on the Tanana River, Alaska. *Can. J.
641 For. Res.* 40, 1273–1287. doi: 10.1139/X10-094](#)

642 Hopkins, D. M., Karlstrom, T. N. V., Black, R. F., Williams, J. R., Pewe, T. L., Fernald, A. T., and Muller, E. H.
643 1955: Permafrost and ground water in Alaska. U.S. Geological Survey Professional Paper 264-F.

644 [Huang, Q., Ma, N., & Wang, P. \(2022\). Faster increase in evapotranspiration in permafrost-dominated basins in the](#)
645 [warming Pan-Arctic. *Journal of Hydrology*, 615, 128678. <https://doi.org/10.1016/j.jhydrol.2022.128678>](#)

646 Jafarov, E. E., Coon, E. T., Harp, D. R., Wilson, C. J., Painter, S. L., Atchley, A. L., and Romanovsky, V. E. 2018:
647 Modelling the role of preferential snow accumulation in through talik development and hillslope groundwater flow in
648 a transitional permafrost landscape. *Environmental Research Letters*, 13: 105006, doi: [https://doi.org/10.1088/1748-](https://doi.org/10.1088/1748-9326/aadd30)
649 [9326/aadd30](https://doi.org/10.1088/1748-9326/aadd30).

650 [Jessen, Søren, Hanne D. Holmslykke, Kristine Rasmussen, Niels Richardt, and Peter E. Holm. 2014. "Hydrology and](#)
651 [Pore Water Chemistry in a Permafrost Wetland, Ilulissat, Greenland." *Water Resources Research* 50 \(6\): 4760–74.](#)
652 <https://doi.org/10.1002/2013WR014376>.

653 Kinniburgh, D., and Cooper, D. 2011: PhreePlot: Creating Graphical Output with Phreeqc.

654 Koch, J. C., Runkel, R. L., Striegl, R., and McKnight, D. M. 2013: Hydrologic controls on the transport and cycling
655 of carbon and nitrogen in a boreal catchment underlain by continuous permafrost. *Journal of Geophysical Research:*
656 *Biogeosciences*, 118: 698–712, doi: <https://doi.org/10.1002/jgrg.20058>.

657 Kokelj, S. V., and Jorgenson, M. T. 2013: Advances in Thermokarst Research. *Permafrost and Periglacial Processes*,
658 24: 108–119, doi: <https://doi.org/10.1002/ppp.1779>.

659 Kurylyk and Walvoord, 2021 Kurylyk, B.L. and Walvoord, M.A., 2021. Permafrost Hydrogeology. In *Arctic*
660 *Hydrology, Permafrost and Ecosystems* (pp. 493-523). Springer, Cham.

661 [Langford, Z. L., Kumar, J., Hoffman, F. M., Breen, A. L., & Iversen, C. M. \(2019\). Arctic vegetation mapping using](#)
662 [unsupervised training datasets and convolutional neural networks. *Remote Sensing*, 11\(1\), 1–23.](#)
663 <https://doi.org/10.3390/rs11010069>

664 Lara, M. J., Nitze, I., Grosse, G., and McGuire, A. D. 2018: Tundra landform and vegetation productivity trend maps
665 for the Arctic Coastal Plain of northern Alaska. *Scientific Data*, 5: 1–10, doi: <https://doi.org/10.1038/sdata.2018.58>.

666 Léger, E., Dafflon, B., Robert, Y., Ulrich, C., Peterson, J. E., Biraud, S. C., ... Hubbard, S. S. 2019: A distributed
667 temperature profiling method for assessing spatial variability in ground temperatures in a discontinuous permafrost
668 region of Alaska. *The Cryosphere*, 13: 2853–2867, doi: <https://doi.org/10.5194/tc-13-2853-2019>.

669 Liljedahl, A. K., Boike, J., Daanen, R. P., Fedorov, A. N., Frost, G. V., Grosse, G., ... Zona, D. 2016: Pan-Arctic ice-
670 wedge degradation in warming permafrost and its influence on tundra hydrology. *Nature Geoscience*, 9: 312–318,
671 doi: <https://doi.org/10.1038/ngeo2674>.

672 [McCaully, R. E., Arendt, C. A., Newman, B. D., Salmon, V. G., Heikoop, J. M., Wilson, C. J., Sevanto, S., Wales, N.](#)
673 [A., Perkins, G. B., Marina, O. C., and Wulfschleger, S. D.: High nitrate variability on an Alaskan permafrost hillslope](#)
674 [dominated by alder shrubs. *The Cryosphere*, 16, 1889–1901, <https://doi.org/10.5194/tc-16-1889-2022>, 2022.](#)

675 [McCaully, R. E., Arendt, C. A., Newman, B. D., Heikoop, J. M., Wilson, C. J., Sevanto, S., ... Wulfschleger, S. D. In](#)
676 [Review.: High Temporal and Spatial Nitrate Variability on an Alaskan Hillslope Dominated by Alder Shrubs. *The*](#)
677 [Cryosphere.](#)

678 McClelland, J. W., Holmes, R. M., Peterson, B. J., Raymond, P. A., Striegl, R. G., Zhulidov, A. V., ... Griffin, C. G.
679 2016: Particulate organic carbon and nitrogen export from major Arctic rivers. *Global Biogeochemical Cycles*, 30:
680 629–643, doi: <https://doi.org/10.1002/2015GB005351>.

681 [Mitchell, J. S., and Ruess, R. W. \(2009\). N2 fixing alder \(*Alnus viridis* spp. *fruticosa*\) effects on soil properties across](#)
682 [a secondary successional chronosequence in interior Alaska. *Biogeochemistry* 95, 215–229. doi: 10.1007/s10533-009-](#)
683 [9332-x](#)

684 Mulligan, J. J. 1965: Examination of the Sinuk Iron Deposits Seward Peninsula, Alaska. United States Department of
685 the Interior, 37.

686 Myers-Smith, I. H., Forbes, B. C., Wilmsking, M., Hallinger, M., Lantz, T., Blok, D., ... Hik, D. S. 2011: Shrub
687 expansion in tundra ecosystems: dynamics, impacts and research priorities. *Environmental Research Letters*, 6:
688 045509, doi: <https://doi.org/10.1088/1748-9326/6/4/045509>.

689 [Neff, J. \(2002\). Barium in the Ocean. In *Bioaccumulation in Marine Organisms* \(pp. 79–87\).](#)
690 [Nossov, D. R., Hollingsworth, T. N., Ruess, R. W., and Kielland, K. \(2011\). Development of *Alnus tenuifolia* stands](#)
691 [on an Alaskan floodplain: patterns of recruitment, disease and succession. *J. Ecol.* 99, 621–633. doi: 10.1111/j.1365-](#)
692 [2745.2010.01792.x](#)

693 O'Donnell, J., Douglas, T., Barker, A. and Guo, L., 2021. Changing Biogeochemical Cycles of Organic Carbon,
694 Nitrogen, Phosphorus, and Trace Elements in Arctic Rivers. In *Arctic Hydrology, Permafrost and Ecosystems* (pp.
695 315-348). Springer, Cham.

696 [Patzner, M.S., Kainz, N., Lundin, E., Barczok, M., Smith, C., Herndon, E., Kinsman-Costello, L., Fischer, S., Straub,](#)
697 [D., Kleindienst, S., Kappler, A., Bryce, C., 2022. Seasonal Fluctuations in Iron Cycling in Thawing Permafrost](#)
698 [Peatlands. *Environ. Sci. Technol.* 56, 4620–4631. <https://doi.org/10.1021/acs.est.1c06937>](#)

699 [Park, H., Tanoue, M., Sugimoto, A., Ichiyangi, K., Iwahana, G., & Hiyama, T. \(2021\). Quantitative Separation of](#)
700 [Precipitation and Permafrost Waters Used for Evapotranspiration in a Boreal Forest: A Numerical Study Using Tracer](#)
701 [Model. *Journal of Geophysical Research: Biogeosciences*, 126\(12\). <https://doi.org/10.1029/2021JG006645>](#)

702 Parkhurst, D., and Appelo, C. A. J. 2013: Description of input and examples for PHREEQC version 3: a computer
703 program for speciation, batch-reaction, one-dimensional transport, and inverse geochemical calculations (USGS
704 Numbered Series No. 6-A43). Reston, VA: U.S. Geological Survey.

705 Perdrial, J. N., Perdrial, N., Vazquez-Ortega, A., Porter, C., Leedy, J., and Chorover, J. 2014: Experimental
706 Assessment of Passive Capillary Wick Sampler Suitability for Inorganic Soil Solution Constituents. *Soil Science*
707 *Society of America Journal*, 78: 486–495, doi: <https://doi.org/10.2136/sssaj2013.07.0279>.

708 Petrone, K. C., Hinzman, L. D., Shibata, H., Jones, J. B., and Boone, R. D. 2007: The influence of fire and permafrost
709 on sub-arctic stream chemistry during storms. *Hydrological Processes*, 21: 423–434, doi:
710 <https://doi.org/10.1002/hyp.6247>.

711 Philben, M., Taş, N., Chen, H., Wullschlegel, S. D., Kholodov, A., Graham, D. E., and Gu, B. 2020: Influences of
712 hillslope biogeochemistry on anaerobic soil organic matter decomposition in a tundra watershed. *Journal of*
713 *Geophysical Research: Biogeosciences*, n/a: e2019JG005512, doi: <https://doi.org/10.1029/2019JG005512>.

Formatted: Normal

714 Philben, M., Zheng, J., Bill, M., Heikoop, J. M., Perkins, G., Yang, Z., ... Gu, B. 2019: Stimulation of anaerobic
715 organic matter decomposition by subsurface organic N addition in tundra soils. *Soil Biology and Biochemistry*, 130:
716 195–204, doi: <https://doi.org/10.1016/j.soilbio.2018.12.009>.

717 Prowse, T., Bring, A., Mård, J., and Carmack, E. 2015: Arctic Freshwater Synthesis: Introduction. *Journal of*
718 *Geophysical Research: Biogeosciences*, 120: 2121–2131, doi: <https://doi.org/10.1002/2015JG003127>.

719 Prowse, T., Bring, A., Mård, J., Carmack, E., Holland, M., Instanes, A., ... Wrona, F. J. 2015: Arctic Freshwater
720 Synthesis: Summary of key emerging issues. *Journal of Geophysical Research: Biogeosciences*, 120: 1887–1893, doi:
721 <https://doi.org/10.1002/2015JG003128>.

722 R Core Team. 2020: R: A Language and Environment for Statistical Computing. Vienna, Austria: R Foundation for
723 Statistical Computing. Retrieved from <https://www.R-project.org/>.

724 [Raudina, Tatiana V., Sergey V. Loiko, Artyom G. Lim, Ivan V. Krickov, Liudmila S. Shirokova, Georgy I. Istigechev,](#)
725 [Daria M. Kuzmina, Sergey P. Kulizhsky, Sergey N. Vorobyev, and Oleg S. Pokrovsky. 2017. "Dissolved Organic](#)
726 [Carbon and Major and Trace Elements in Peat Porewater of Sporadic, Discontinuous, and Continuous Permafrost](#)
727 [Zones of Western Siberia." *Biogeosciences* 14 \(14\): 3561–84. <https://doi.org/10.5194/bg-14-3561-2017>.](#)

728 [Raynolds, M.K.; Walker, D.A.; Maier, H.A. Plant community-level mapping of arctic Alaska based on the](#)
729 [Circumpolar Arctic Vegetation Map. *Phytocoenologia* 2005, 35, 821–848.](#)

730 [Raynolds, M. K., Walker, D. A., Balsler, A., Bay, C., Campbell, M., Cherosov, M. M., et al. \(2019\). A raster version](#)
731 [of the Circumpolar Arctic Vegetation Map \(CAVM\). *Remote Sensing of Environment*, 232,](#)
732 <https://doi.org/10.1016/j.rse.2019.111297>

733 Romanovsky, V., Cable, W., and Dolgikh, K. 2020a: Soil Temperature and Moisture, Kougarak Road Mile Marker
734 64, Seward Peninsula, Alaska, beginning 2016 [Data set], doi: <https://doi.org/10.5440/1581586>.

735 Romanovsky, V., Cable, W., and Dolgikh, K. 2020b: Soil Temperature and Moisture, Kougarak Road Mile Marker
736 64, Seward Peninsula, Alaska, beginning 2016 [Data set], doi: <https://doi.org/10.5440/1581586>.

737 Romanovsky, V., Cable, W., and Dolgikh, K. 2020c: Soil Temperature and Moisture, Teller Road Mile Marker 27,
738 Seward Peninsula, Alaska, beginning 2016 [Data set], doi: <https://doi.org/10.5440/1581437>.

739 Romanovsky, V., Cable, W., and Dolgikh, K. 2020d: Soil Temperature and Moisture, Teller Road Mile Marker 27,
740 Seward Peninsula, Alaska, beginning 2016 [Data set], doi: <https://doi.org/10.5440/1581437>.

741 Rowland, J. C., Jones, C. E., Altmann, G., Bryan, R., Crosby, B. T., Hinzman, L. D., ... Geernaert, G. L. 2010: Arctic
742 Landscapes in Transition: Responses to Thawing Permafrost. *Eos, Transactions American Geophysical Union*, 91:
743 229–230, doi: <https://doi.org/10.1029/2010EO260001>.

744 [Ruess, R. W., Anderson, M. D., Mcfarland, J. M., Kielland, K., Olson, K., and Taylor, D. L. \(2013\). Ecosystem-level](#)
745 [consequences of symbiont partnerships in an N-fixing shrub from interior Alaskan floodplains. *Ecol. Monogr.* 83,](#)
746 [177–194. doi: 10.1890/12-0782.1](https://doi.org/10.1890/12-0782.1)

747 Salmon, V. G., Breen, A. L., Kumar, J., Lara, M. J., Thornton, P. E., Wulfschleger, S. D., and Iversen, C. M. 2019:
748 Alder Distribution and Expansion Across a Tundra Hillslope: Implications for Local N Cycling. *Frontiers in Plant*
749 *Science*, 10, doi: <https://doi.org/10.3389/fpls.2019.01099>.

750 Schuur, E. A. G., McGuire, A. D., Schädel, C., Grosse, G., Harden, J. W., Hayes, D. J., ... Vonk, J. E. 2015: Climate
751 change and the permafrost carbon feedback. *Nature*, 520: 171–179, doi: <https://doi.org/10.1038/nature14338>.

752 Shaver, G. R., Billings, W. D., Chapin, F. S., Giblin, A. E., Nadelhoffer, K. J., Oechel, W. C., and Rastetter, E. B.
753 1992: Global Change and the Carbon Balance of Arctic Ecosystems. *BioScience*, 42: 433–441, doi:
754 <https://doi.org/10.2307/1311862>.

755 Shogren, A. J., Zarnetske, J. P., Abbott, B. W., Iannucci, F., Frei, R. J., Griffin, N. A., and Bowden, W. B. 2019:
756 Revealing biogeochemical signatures of Arctic landscapes with river chemistry. *Scientific Reports*, 9: 1–11, doi:
757 <https://doi.org/10.1038/s41598-019-49296-6>.

758 [Sjöberg, Y., Jan, A., Painter, S. L., Coon, E. T., Carey, M. P., O'Donnell, J. A., & Koch, J. C. \(2021\). Permafrost](#)
759 [Promotes Shallow Groundwater Flow and Warmer Headwater Streams. *Water Resources Research*, 57\(2\).](#)
760 <https://doi.org/10.1029/2020WR027463>

761 Smith, L. C., Sheng, Y., MacDonald, G. M., and Hinzman, L. D. 2005: Disappearing Arctic Lakes. *Science*, 308:
762 1429–1429, doi: <https://doi.org/10.1126/science.1108142>.

763 Sparks, D. L. 2003: *Environmental soil chemistry* (2nd ed). Amsterdam ; Boston, : Academic Press, 352 pp.

764 Spence, C., Kokelj, S., McCluskie, M., and Hedstrom, N. 2015: Impacts of Hydrological and Biogeochemical Process
765 Synchrony Transcend Scale. In *AGU Fall Meeting Abstracts* (Vol. 2015).

766 Sturm, M., Racine, C., and Tape, K. 2001: Increasing shrub abundance in the Arctic. *Nature*, 411: 546–547, doi:
767 <https://doi.org/10.1038/35079180>.

768 [Sulman, B. N., Salmon, V. G., Iversen, C. M., Breen, A. L., Yuan, F., & Thornton, P. E. \(2021\). Integrating arctic](#)
769 [plant functional types in a land surface model using above- and belowground field observations. *Journal of Advances*](#)
770 [in Modeling Earth Systems](#), 13, e2020MS002396. <https://doi.org/10.1029/2020MS002396>

771 Tape, K. D., Hallinger, M., Welker, J. M., and Ruess, R. W. 2012: Landscape Heterogeneity of Shrub Expansion in
772 Arctic Alaska. *Ecosystems*, 15: 711–724, doi: <https://doi.org/10.1007/s10021-012-9540-4>.

773 Tape, K., Sturm, M., and Racine, C. 2006: The evidence for shrub expansion in Northern Alaska and the Pan-Arctic.
774 *Global Change Biology*, 12: 686–702, doi: <https://doi.org/10.1111/j.1365-2486.2006.01128.x>.

775 Till, A. B., Dumoulin, J. A., Weldon, M. B., and Bleick, H. A. 2011: Bedrock geologic map of the Seward Peninsula,
776 Alaska, and accompanying conodont data. US Department of the Interior, US Geological Survey.

777 Uren, N. C. 2018: Calcium oxalate in soils, its origins and fate – a review. *Soil Research*, 56: 443, doi:
778 <https://doi.org/10.1071/SR17244>.

779 Vonk, J. E., Tank, S. E., Bowden, W. B., Laurion, I., Vincent, W. F., Alekseychik, P., ... Wickland, K. P. 2015:
780 Reviews and syntheses: Effects of permafrost thaw on Arctic aquatic ecosystems. *Biogeosciences*, 12: 7129–7167,
781 doi: <https://doi.org/10.5194/bg-12-7129-2015>.

782 Vonk, J. E., Tank, S. E., and Walvoord, M. A. 2019: Integrating hydrology and biogeochemistry across frozen
783 landscapes. *Nature Communications*, 10: 1–4, doi: <https://doi.org/10.1038/s41467-019-13361-5>.

784 [Walker, D. A., Breen, A. L., Druckenmiller, L. A., Wirth, L. W., Fisher, W., Reynolds, M. K., Sibik, J., Walker, M.](#)
785 [D., Hennekens, S., Boggs, K., Boucher, T., Buchhorn, M., Bultmann, H., Cooper, D. J., Daniels, F. J. A., Davidson,](#)
786 [S. J., Ebersole, J. J., Elmendorf, S. C., Epstein, H. E., Gould, W. A., Hollister, R. D., Iversen, C. M., Jorgenson, M.](#)

787 [T., Kade, A., Lee, M. T., MacKenzie, W. H., Peet, R. K., Peirce, J. L., Schickhoff, U., Sloan, V. L., Talbot, S. S.,](#)
788 [Tweedie, C. E., Villarreal, S., Webber, P. J., and Zona, D.: The Alaska Arctic Vegetation Archive \(AVA-AK\),](#)
789 [Phytocoenologia, 46, 221–229, <https://doi.org/10.1127/phyto/2016/0128>, 2016.](#)

790 Wallenberger, F. T., and Bingham, P. A. 2009: *Fiberglass and Glass Technology: Energy-Friendly Compositions and*
791 *Applications*. Springer Science & Business Media, 479 pp.

792 Walvoord, M. A., and Kurylyk, B. L. 2016: Hydrologic Impacts of Thawing Permafrost—A Review. *Vadose Zone*
793 *Journal*, 15, doi: <https://doi.org/10.2136/vzj2016.01.0010>.

794 Weiss, M., Hobbie, S. E., & Gettel, G. M. (2005). Contrasting Responses of Nitrogen-Fixation in Arctic Lichens to
795 Experimental and Ambient Nitrogen and Phosphorus Availability. *Arctic, Antarctic, and Alpine Research*, 37(3), 396–
796 401. [https://doi.org/10.1657/1523-0430\(2005\)037\[0396:CRONIA\]2.0.CO;2](https://doi.org/10.1657/1523-0430(2005)037[0396:CRONIA]2.0.CO;2)

797 Wilson, C., Bolton, R., Busey, R., Lathrop, E., and Dann, J. 2019: End-of-Winter Snow Depth, Temperature, Density
798 and SWE Measurements at Kougarok Road Site, Seward Peninsula, Alaska, 2018 [Data set], doi:
799 <https://doi.org/10.5440/1593874>.

800 Wilson, C., Bolton, R., Busey, R., Lathrop, E., Dann, J., and Charsley-Groffman, L. 2019: End-of-Winter Snow Depth,
801 Temperature, Density and SWE Measurements at Teller Road Site, Seward Peninsula, Alaska, 2016–2018 [Data set],
802 doi: <https://doi.org/10.5440/1592103>.

803 Wilson, C., Dann, J., Bolton, R., Charsley-Groffman, L., Jafarov, E., Musa, D., and Wulschleger, S. 2021: In Situ
804 Soil Moisture and Thaw Depth Measurements Coincident with Airborne SAR Data Collections, Barrow and Seward
805 Peninsulas, Alaska, 2017 [Data set], doi: <https://doi.org/10.5440/1423892>.

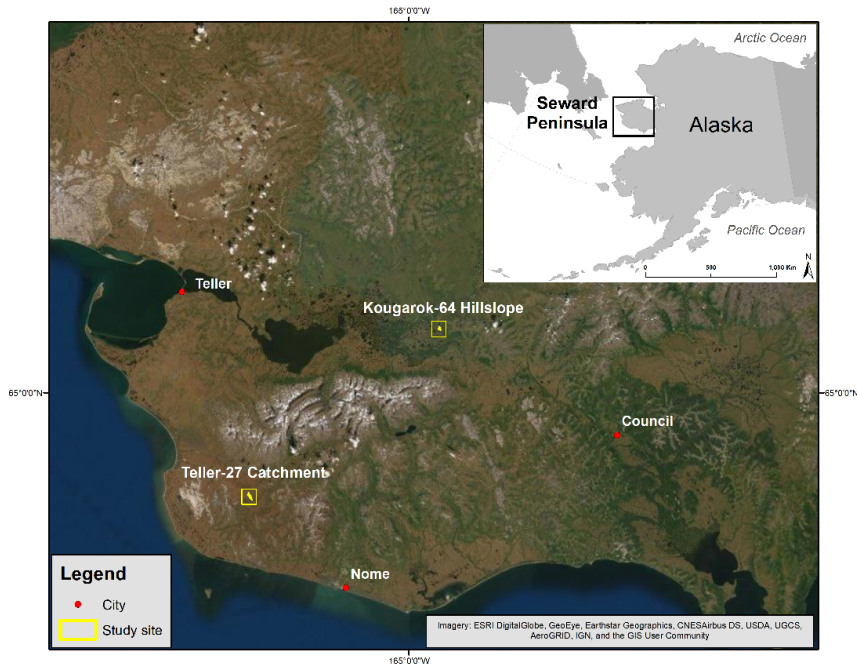
806 Wrona, F. J., Johansson, M., Culp, J. M., Jenkins, A., Mård, J., Myers-Smith, I. H., ... Wookey, P. A. 2016: Transitions
807 in Arctic ecosystems: Ecological implications of a changing hydrological regime. *Journal of Geophysical Research:*
808 *Biogeosciences*, 121: 650–674, doi: <https://doi.org/10.1002/2015JG003133>.

809 [Wulschleger, S. D., Epstein, H. E., Box, E. O., Euskirchen, E. S., Goswami, S., Iversen, C. M., et al. \(2014\). Plant](#)
810 [functional types in earth system models: past experiences and future directions for application of dynamic vegetation](#)
811 [models in high-latitude ecosystems. *Ann. Bot.* 114, 1–16. doi: 10.1093/aob/mcu077](#)

812 Yang, D., Meng, R., Morrison, B. D., McMahon, A., Hantson, W., Hayes, D. J., ... Serbin, S. P. 2020: A Multi-Sensor
813 Unoccupied Aerial System Improves Characterization of Vegetation Composition and Canopy Properties in the Arctic
814 Tundra. *Remote Sensing*, 12: 2638, doi: <https://doi.org/10.3390/rs12162638>.

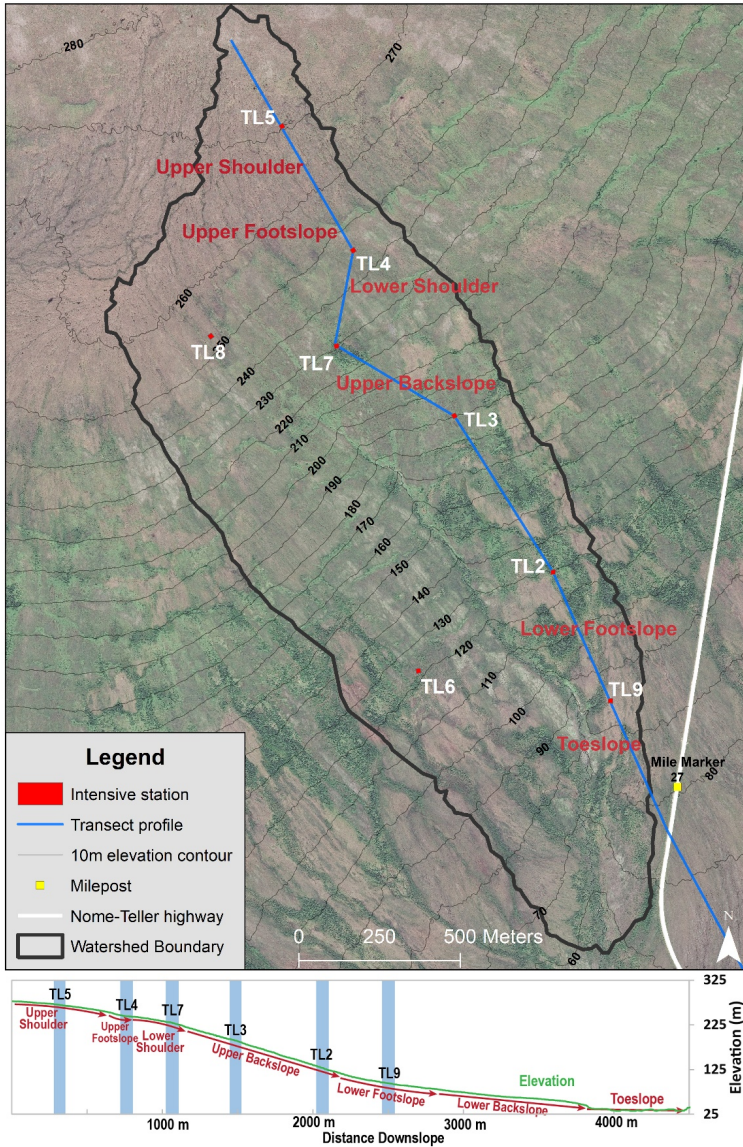
815 [Yang, D., et al. "Landscape-Scale Characterization of Arctic Tundra Vegetation Composition, Structure, and Function](#)
816 [with a Multi-Sensor Unoccupied Aerial System." *Environmental Research Letters* 16 \(8\), 085005 \(2021\).](#)
817 <https://doi.org/10.1088/1748-9326/ac1291>.

818

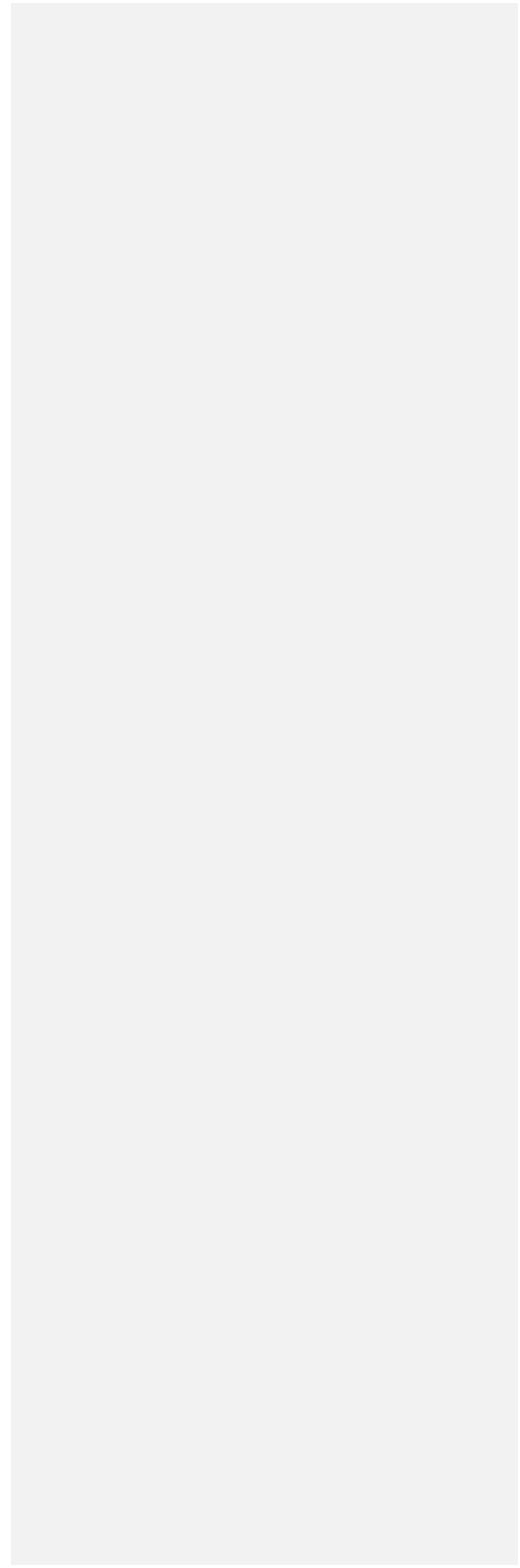


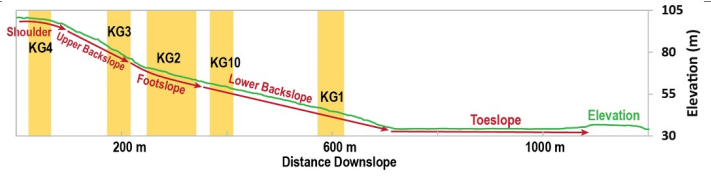
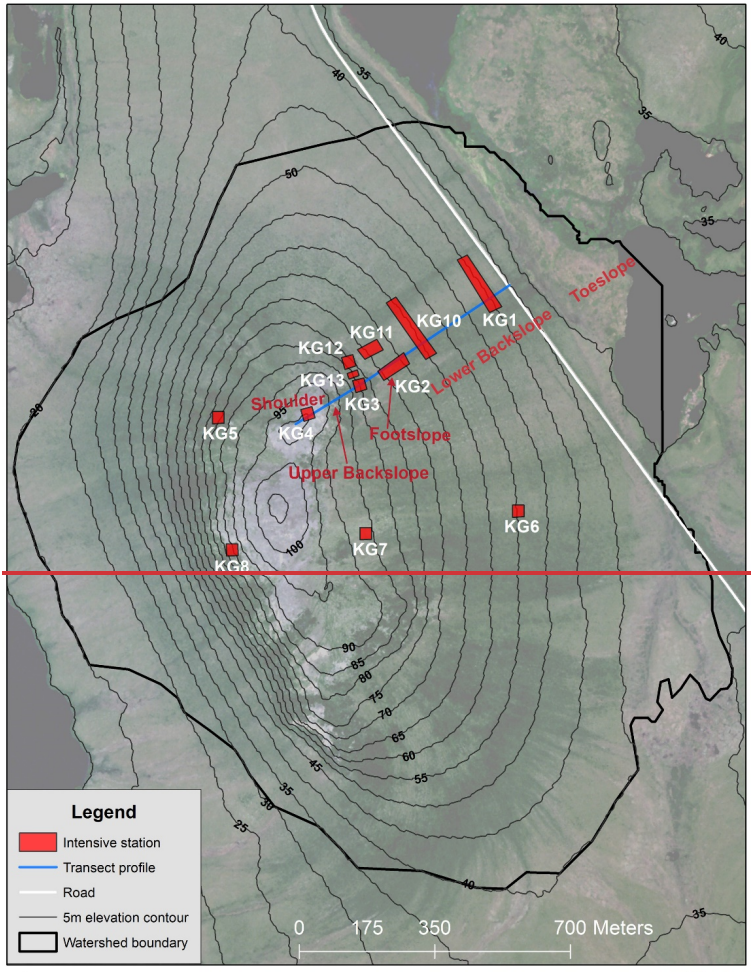
820
821 **Figure 1. Location of the Teller and Kougarok field sites with respect to the municipalities of Teller, Nome, and Council.**
822 **All are located on the Seward Peninsula in northwestern Alaska. RGB composite imagery from the 8-band WorldView-2**
823 **imagery obtained on July 14, 2017 at 1.5 m resolution downloaded from the DigitalGlobe website**
824 **(<https://www.digitalglobe.com/>).**

825
826

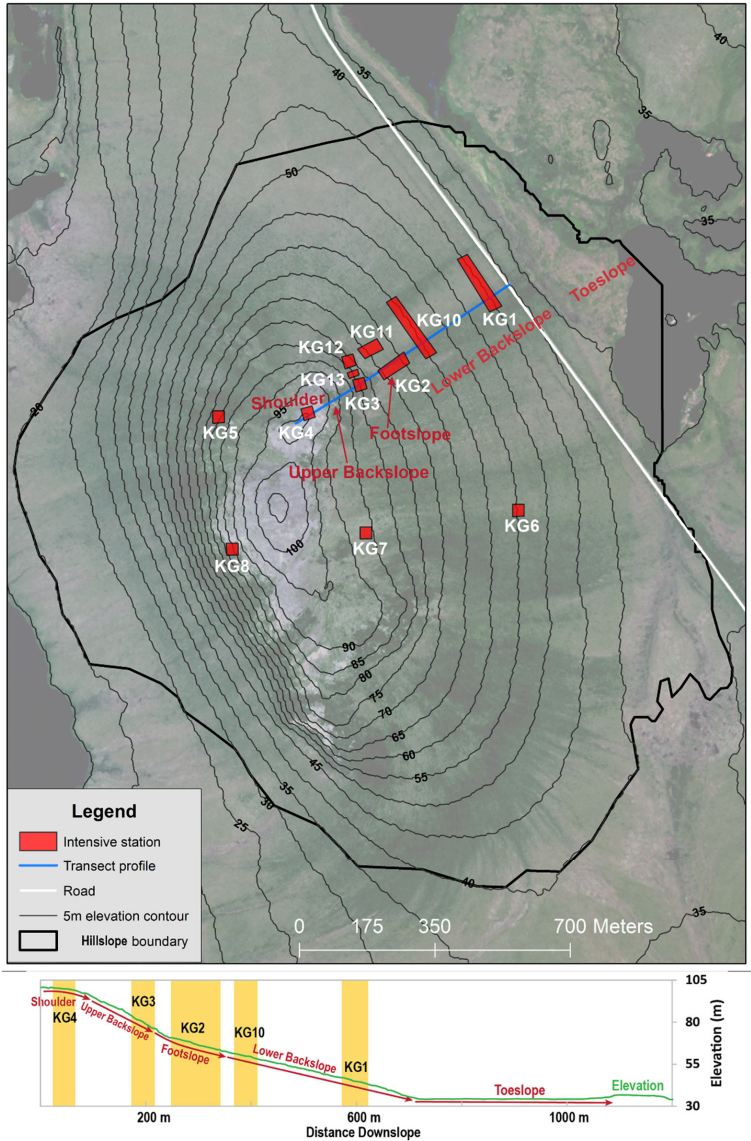


827
 828 Figure 2. Topographic map of Teller. Station areas are shown as red polygons and the topographic station transect is given
 829 as a solid blue line. The hillslope transect elevation profile is given below the map in green, with stations along the transect
 830 in blue and hillslope positions noted with red arrows and text. RGB composite imagery from the 8-band WorldView-2
 831 imagery obtained on July 27, 2011 at 1.5 m resolution downloaded from the DigitalGlobe website
 832 (<https://www.digitalglobe.com/>).

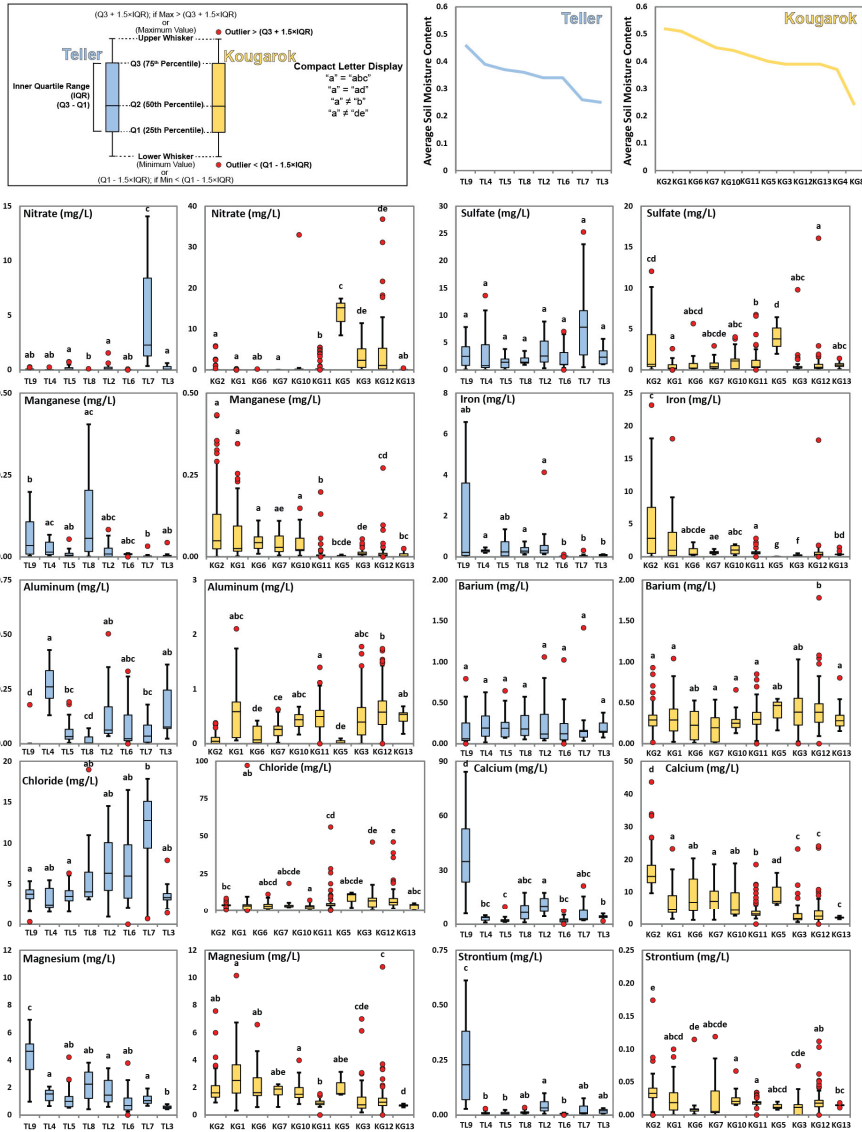




834

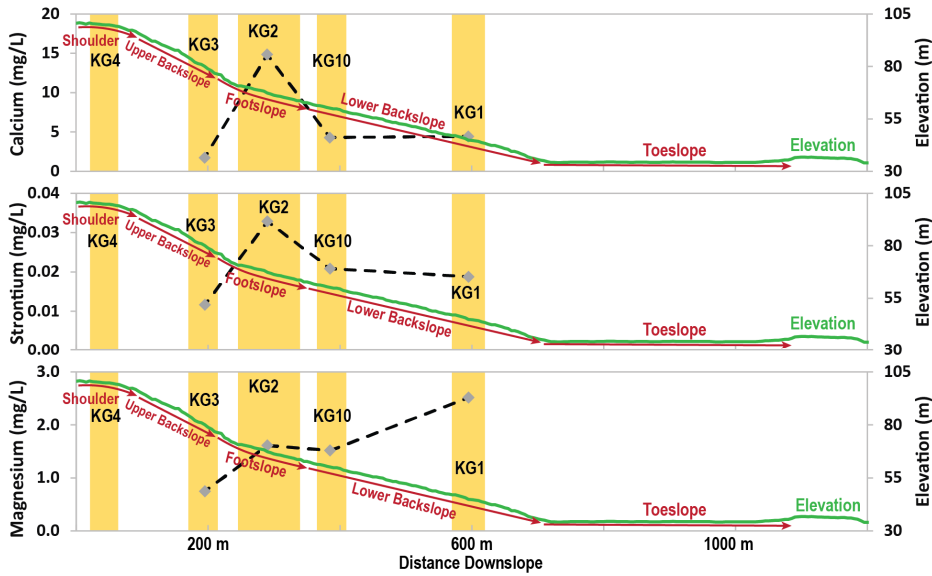
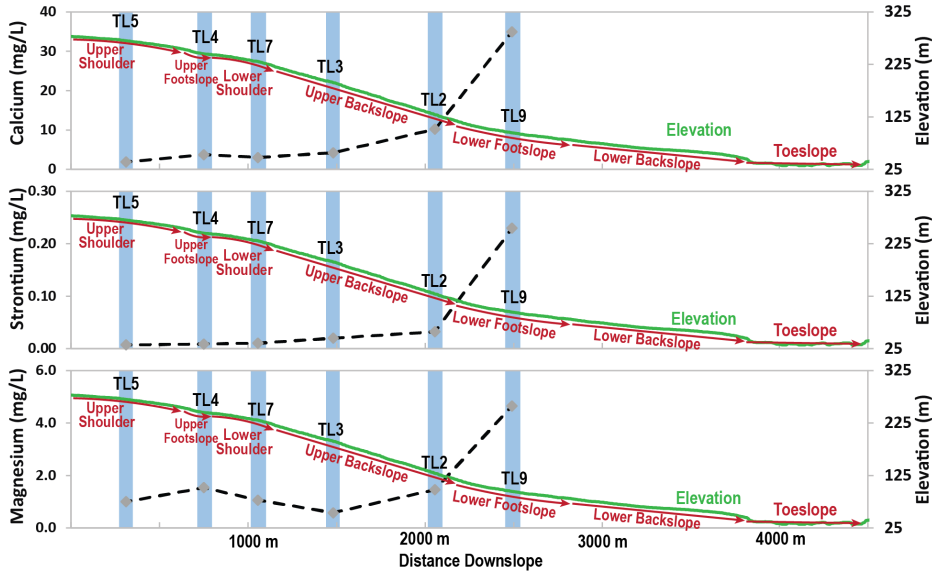


835
 836 Figure 3. Topographic map of Kougarok. Station areas are shown as red polygons and the station transect is given as a
 837 solid blue line. The transect elevation profile is given below the map in green, with stations along the transect in yellow and
 838 hillslope positions noted with red arrows and text. RGB composite imagery from the 8-band WorldView-2 imagery obtained
 839 on July 14, 2017 at 1.5 m resolution downloaded from the DigitalGlobe website (<https://www.digitalglobe.com/>).



841
 842 **Figure 4.** Mean COI concentrations at Teller (blue) and Kougarok (yellow) stations. Stations are arranged (left to right) by
 843 soil moisture content determined by P-Band SAR (top right). Boxplots show the first, second, and third data quartiles, with
 844 box whiskers representing either 150% of the inner quartile range (IQR), or the maximum or minimum value, when that
 845 value was less than 1.5×IQR. Red circles represent data points outside of the 1.5×IQR whiskers (i.e. outliers). Note that the
 846 concentration scales on the Teller and Kougarok plots often differ.

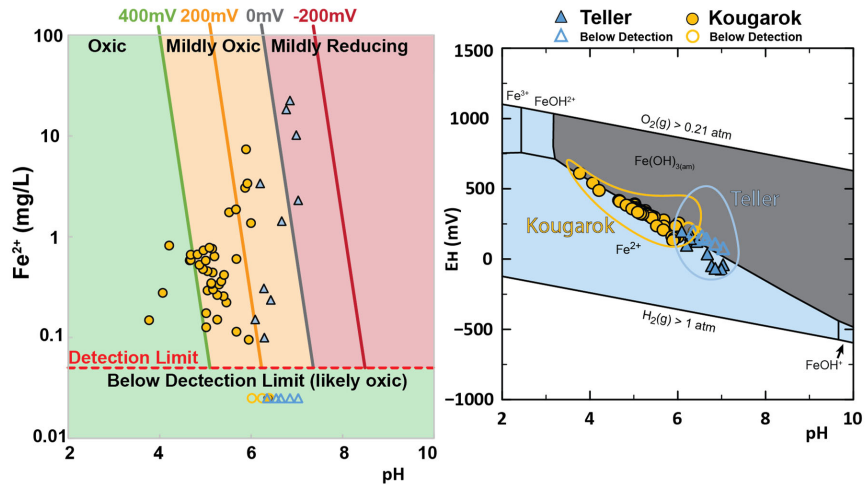
847



848

849 Figure 5. Median (50th percentile) concentrations (grey diamonds with dashed black lines) of Ca, Sr, and Mg, with distance
 850 downslope at Teller (blue) and Kougarak (yellow) along topographic transects; areas of stations are indicated by blue
 851 and yellow colouring, respectively. The elevation profiles of the hillslopes are plotted in green, on separate y-axes (right axes).
 852 Topographic regions of both catchments are indicated by red arrows along the elevation gradient.

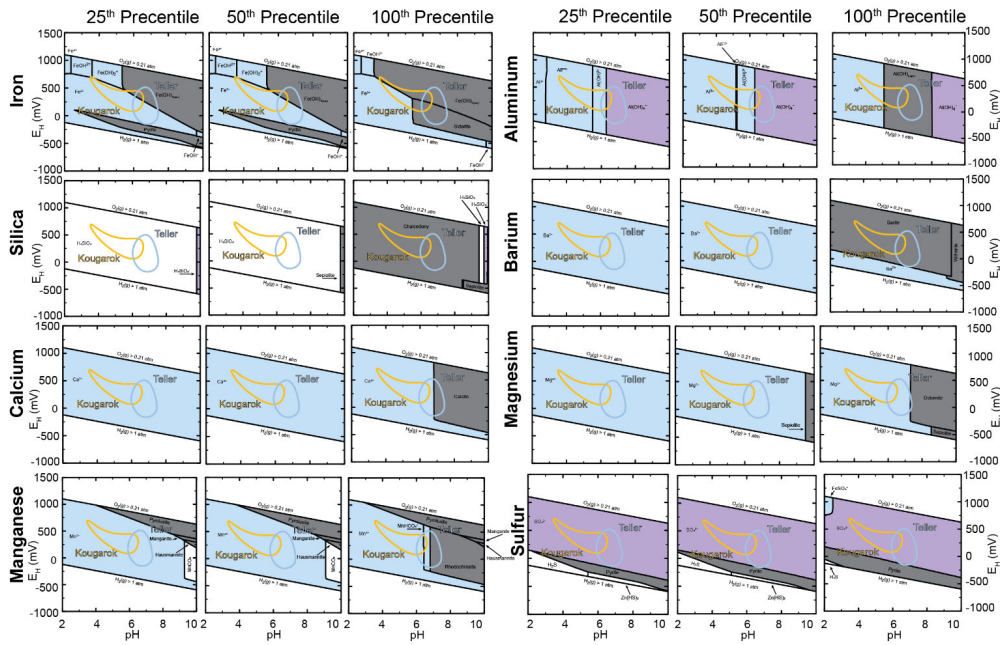
853



854

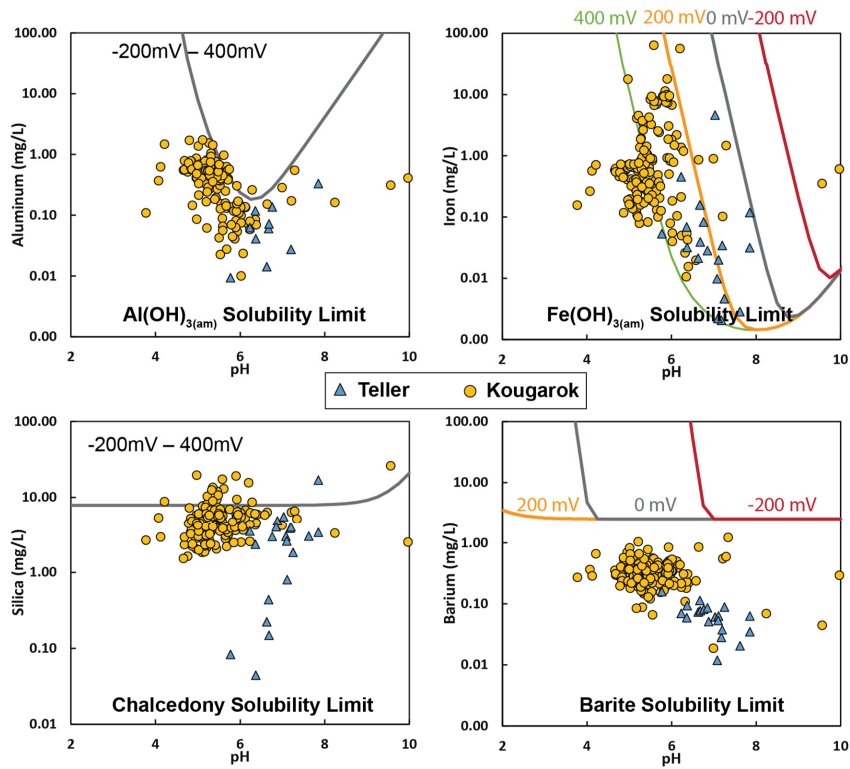
855 Figure 6. Left: Model-predicted Fe²⁺ concentrations in saturated solutions of Fe(OH)_{3(am)} at fixed E_H conditions of 400 mV
856 (green), 200 mV (orange), 0 mV (grey), and -200 mV (red), compared with field concentrations of Fe²⁺ at Teller (red circles)
857 and Kougarok (yellow circles). Right: Fe predominance diagram, showing the dominant specie of Fe under a range of
858 Eh/pH conditions. Eh/pH regions relevant to Teller and Kougarok are outlined in blue and yellow, respectively. Samples
859 with Fe²⁺ concentrations below the detection limit are given as colour coordinated open circles set at 0.025 mg·L⁻¹ (half the
860 detection limit) in both sides of the figure.

861



862
 863 **Figure 7. Eh/pH diagrams for key species that indicated possible mineral formation under the Eh/pH conditions present at**
 864 **either Teller or Kougarok. The Eh and pH conditions observed at Teller and Kougarok are overlaid as blue and yellow**
 865 **lines, respectively. Mineral species (solids) are shown in grey, cations are shown in blue, anions are shown in purple,**
 866 **neutral species are shown in white. Predominance diagrams were created in PhreePlot using the phreeqc.dat database, with**
 867 **inorganic carbonate reduction to methane “turned off.”**

868



869

870

871

Figure 8. Modelled solute concentrations in solutions saturated with $\text{Al(OH)}_{3(\text{am})}$, $\text{Fe(OH)}_{3(\text{am})}$, chalcedony, and barite, with respect to pH (x-axis) and E_H (model lines), overlaid with observed solute concentrations.

872

873 **910. Tables**

874 **Table 1. Teller Station Physical Characteristics**

	Hillslope Position	Vegetation				Relative wetness			Permafrost			
		Vegetation type	Average (maximum) canopy height (cm)	Dominant PFT	Low to tall shrub cover	Average TDR soil moisture (VMC)	Average P-band SAR (VMC)	Average snow depth (cm)	Average Ground Temperature (°C)	Permafrost Extent	Average (maximum) thaw depth (cm)	
TL9	Lower Foothslope		2834 (41)	Graminoid Bryophyte	44%	10%	NA	0.46	68.4	0	Marginal	101 (>20)
TL5	Upper Shoulder	Wetland complex	1234 (45)	Graminoid	45%	7%	0.55	0.37	103.3	-0.45	Near-surface	97' (>114')
TL8	Upper Foothslope		47 (34)	Bryophyte	33%	20%	0.55	0.36	77.7	-0.6		69' (>120)
TL3	Upper Backslope	Cassiope dwarf shrub	913 (23)	Evergreen dwarf shrub	47%	124%	NA	0.25	62.1	2.2	None/ deep	72' (82')
TL4	Upper Foothslope	tundra	408 (14)		58%	4%	0.35	0.39	89.5	0.5	Marginal	40' (70')
TL2	Upper Backslope	Mesic willow shrubland	8432 (141)	Deciduous low to tall shrub (willow)	44%	44%	0.4	0.34	124	2.4	None/ deep	75' (>120)
TL7	Lower Shoulder		468-151 (189)		37%	37%	0.46	0.26	128.8	2.4		51' (66')
TL6	Upper Backslope	Willow-birch tundra	7464 (115)	ForbDeciduous-low shrub (willow & birch)	23%	32%	0.38	0.34	86.4	1.2	None/ deep	67' (102')

Formatted Table

875

876 PFT – plant functional type; dwarf shrub (height <40 cm), low shrub (height 40-200 cm), low to tall shrub (height 40 to >200 cm tall).
 877 Deciduous shrub PFT classes identify the dominant species in the plant community as either willow or willow and birch. There is no alder at
 878 the Teller site. Low to tall shrub cover represents the sum of deciduous low shrubs, deciduous low to potentially tall willow and birch, and
 879 deciduous low to tall alder.

880 ¹Single point soil moisture measurements. Data are more accurate than P-band SAR but represent a much smaller spatial scale.

881 ²P-band SAR has 30m resolution.

882 ³Resistive layer was rock; all others are permafrost. A temperature probe was used to determine if the resistive layer was permafrost (≤0 °C)
 883 or rock (>2 °C). Thaw depth is an average of 4 measurements from the vegetation plot corners within the IS and was measured at the end of
 884 the growing season.
 885

886 **Table 2. Kougarok Station Physical Characteristics**

	Hillslope Position	Vegetation				Relative wetness			Permafrost			
		Vegetation type	Average (maximum) canopy height (cm)	Dominant PFT		Low to tall shrub cover	Average TDR soil moisture (VMC)	Average P-band SAR (VMC)	Average snow depth (cm)	Average Ground Temperature (°C)	Permafrost Extent	Average (maximum) thaw depth (cm)
KG3	Upper Backslope	Alder shrubland	204 (265)	Deciduous low to tall shrub (alder)	30%	53% ¹	0.19	0.39	131.3	-0.01	Near-surface	48 [†] (53r)
KG12	Footslope		NA	NA	NA	NA	0.30*	0.39	NA	NA		NA*
KG1	Lower Backslope		60 (90)	Deciduous low shrub (alder, willow & birch)	31%	44% ¹	NA	0.51	83.4	-2.5		61 (68)
KG2	Footslope	Alder savanna in tussock tundra	48 (73)	Graminoid	30%	42% ¹	0.63	0.52	102.3	-1.2	Near-surface	75 (89)
KG6	Lower Backslope		24 (61)	Graminoid	46%	17% ¹	0.36	0.48	66.2	-2.2		58 (62)
KG10	Lower Backslope		NA	NA	NA	NA	NA*	0.44	71.4	NA		NA*
KG11	Footslope		NA	NA	NA	NA	0.59*	0.42	NA	NA		NA*
KG7	Upper Backslope	Tussock-lichen tundra	20 (22)	Graminoid	34%	14% ¹	0.51	0.45	54.7	-2.1	Near-surface	76 (100)
KG4	Shoulder	Dryas-lichen shrub tundra	6 (12)	Evergreen dwarf shrub	62%	1% ¹	NA	0.37	NA	-1.9	Near-surface	0 [†] (0 [†])
KG13	Upper Backslope		NA	NA	NA	NA	0.41*	0.39	92.1	NA		NA*
KG5	Upper Backslope	Willow-birch tundra	62 (137)	Deciduous low shrub (willow & birch)	60%	62% ¹	NA	0.4	178.4	> 0	Deep	88 (96)
KG8	Upper Backslope		45 (120)	Evergreen dwarf shrub	52%	42% ¹	0.23	0.24	85.5	-0.04	Near-surface	44 [†] (58 [†])

Formatted: Centered

Formatted Table

Formatted: Centered

Formatted Table

Formatted: Centered

Formatted: Centered

Formatted Table

Formatted: Centered

Formatted Table

Formatted: Centered

Formatted Table

887
 888 Note: PFT – plant functional type. Deciduous shrub PFT classes identify the dominant species in the community as either willow, alder,
 889 willow and birch, or alder, willow, and birch. Low to tall shrub cover represents the sum of deciduous low shrubs, deciduous low to potentially
 890 tall willow and birch, and deciduous low to tall alder.
 891 ¹Single point soil moisture measurements. Data are more accurate than P-band SAR but represent a much smaller spatial scale.
 892 ²P-band SAR has 30m resolution.
 893 *Average gravimetric water content measurements, corrected to VMC by bulk density.
 894 [†]Resistive layer was rock; all others are permafrost. A temperature probe was used to determine if the resistive layer was permafrost (≤ 0 °C)
 895 or rock (>2 °C). Thaw depth is an average of 4 measurements from the vegetation plot corners within the 1S and was measured at the end of
 896 the growing season.

Table 3. Inter-Site Mann-Whitney U-Test Results

	Teller			Kougarok			z	Site with Higher Median	Effect Size	Difference in Correlation
	n	$\sum R_i$	U_i	n	$\sum R_i$	U_i				
Na	59	3184	14811.5	275	52761.5	1413.5	9.95	Kougarok	0.54	large
F	59	3502	14375.5	273	51776.5	1731.5	9.46	Kougarok	0.52	large
K	59	3882	14113	275	52063	2112	8.92	Kougarok	0.49	medium-large
Si	59	4119	13876.5	275	51826.5	2348.5	8.56	Kougarok	0.47	medium-large
Al	58	4952	12709	275	50659	3241	7.11	Kougarok	0.39	medium
Oxalate	57	4996	12161.5	272	49289.5	3342.5	6.75	Kougarok	0.37	medium
B	59	5429	12566.5	275	50516.5	3658.5	6.62	Kougarok	0.36	medium
Zn	58	5605	12056	275	50006	3894	6.12	Kougarok	0.34	medium
SO ₄	58	13653	3892.5	273	41293.5	11941.5	6.08	Teller	0.33	medium
Fe	58	5958	11703	275	49653	4247	5.60	Kougarok	0.31	medium
Ba	58	6256	11405.5	275	49355.5	4544.5	5.15	Kougarok	0.28	medium
Ti	58	6266	11395.5	275	49345.5	4554.5	5.13	Kougarok	0.28	medium
NO ₂	54	5588	10585.5	272	47713.5	4102.5	5.12	Kougarok	0.28	medium
Li	58	7778	9883	275	47833	6067	2.86	Kougarok	0.16	small-medium
Br	58	8485	9060.5	273	46461.5	6773.5	1.73	Equal	0.09	small
NO ₃	58	8576	8969	273	46370	6865	1.59	Kougarok	0.09	small
Sr	58	8683	8978	275	46928	6972	1.51	Kougarok	0.08	small
PO ₄	54	9659	6460.5	271	43316.5	8173.5	1.36	Equal	0.08	small
Mg	58	10495	7166	275	45116	8784	1.21	Teller	0.07	small
Cr	58	8884	8777	275	46727	7173	1.20	Kougarok	0.07	small
Mn	58	9164	8497	275	46447	7453	0.78	Teller	0.04	small
Cl	58	9221	8266.5	272	45394.5	7509.5	0.57	Kougarok	0.03	small
Ca	58	10016	7645	275	45595	8305	0.50	Teller	0.03	small

900 Table 4. Dominant Environmental Controls on SPW Geochemistry at Teller and Kougarok

Environmental Control	Analytes Affected
Vegetation	NO₃NO₂⁻
Soil Moisture/Redox	NO₃NO₂⁻ , Mn, Fe, SO ₄ (occasionally)
Water/Soil Interactions & Hydrologic Transport	Ca, Mg, Sr
Mineral Solubility	Al, Ba, Si, Fe

Formatted: Subscript

Formatted: Subscript